THE ASTROPHYSICAL JOURNAL, 543:552–576, 2000 November 10

SURVEYS FOR $z > 3$ DAMPED Lyα ABSORPTION SYSTEMS: THE EVOLUTION OF NEUTRAL GAS[1]

LISA J. STORRIE-LOMBARDI
SIRTF Science Center, California Institute of Technology, MS 100-22, Pasadena, CA 91125; lisa@ipac.caltech.edu
AND
ARTHUR M. WOLFE
Department of Physics, and Center for Astrophysics and Space Sciences, University of California at San Diego, La Jolla, CA 92093-0424
Received 2000 March 2; accepted 2000 June 12

ABSTRACT

We have completed spectroscopic observations using LRIS on the Keck 1 telescope of 30 very high redshift quasars, 11 selected for the presence of damped Lyα absorption systems and 19 with redshifts $z > 3.5$ not previously surveyed for absorption systems. We have surveyed an additional 10 QSOs with the Lick 120″ and the Anglo-Australian Telescope. We have combined these with previous data, resulting in a statistical sample of 646 QSOs and 85 damped Lyα absorbers with column densities $N_{\rm H\,I} \geq 2 \times 10^{20}$ atoms cm^{-2} covering the redshift range $0.008 \leq z \leq 4.694$. Four main features of how the neutral gas in the universe evolves with redshift are evident from these data.

1. For the first time, we determine a *statistically significant* steepening in the column density distribution function at redshifts $z > 4.0$ (greater than 99.7% confidence). The steepening of the distribution function is due to both fewer very high column density absorbers ($N_{\rm H\,I} \geq 10^{21}$ atoms cm^{-2}) and more lower column density systems ($N_{\rm H\,I} = 2$–4×10^{20} atoms cm^{-2}).

2. The frequency of very high column density absorbers ($N_{\rm H\,I} \geq 10^{21}$ atoms cm^{-2}) reaches a peak in the redshift range $1.5 < z < 4$, when the universe is 10%–30% of its present age. Although the sample size is still small, the peak epoch appears to be $3.0 \leq z \leq 3.5$. The highest column density absorbers disappear rapidly toward higher redshifts in the range $z = 3.5 \rightarrow 4.7$ and lower redshifts $z = 3.0 \rightarrow 0$. None with column densities $\log N_{\rm H\,I} \geq 21$ have yet been detected at $z > 4$, although we have increased the redshift path surveyed by $\approx 60\%$.

3. With our current data set, the comoving mass density of neutral gas, Ω_g, appears to peak at $3.0 < z < 3.5$, but the uncertainties are still too large to determine the precise shape of Ω_g. The statistics are consistent with a constant value of Ω_g for $2 < z < 4$. There is still tentative evidence for a drop-off at $z > 4$, as indicated by earlier data sets. If we define $R_{g*} \equiv \Omega_g/\Omega_*$, where R_{g*} is the ratio of the peak value of Ω_g to Ω_*, the mass density in galaxies in the local universe, we find values of $R_{g*} = 0.25$–0.5 at $z \sim 3$, depending on the cosmology. For an $\Omega = 1$ universe with a zero cosmological constant, $R_{g*} \approx 0.5$. For an $\Omega = 1$ universe with a positive cosmological constant ($\Omega_\Lambda = 0.7$, $\Omega_M = 0.3$), we find $R_{g*} \approx 0.25$. For a universe with $\Omega_\Lambda = 0$ and $\Omega_M = 0.3$, we find $R_{g*} \approx 0.3$.

4. Ω_g decreases with redshift for the interval $z = 3.5 \rightarrow 0.008$ for our data set, but we briefly discuss new results from Rao & Turnshek for $z < 1.5$ that suggest that Ω_g ($z < 1.5$) may be higher than previously determined.

To make the data in our statistical sample more readily available for comparison with scenarios from various cosmological models, we provide tables that include all 646 QSOs from our new survey and previously published surveys. They list the minimum and maximum redshift defining the redshift path along each line of sight, the QSO emission redshift, and when an absorber is detected, the absorption redshift and measured H I column density.

Subject headings: galaxies: evolution — intergalactic medium — quasars: absorption lines

1. INTRODUCTION

Surveys for damped Lyα absorption systems have been driven historically by the desire to detect galaxies in very early stages of evolution, before most of the gas has turned into stars. Because the gas should be neutral and at high column densities ($N_{\rm H\,I} > 10^{20}$ atoms cm^{-2}), it will leave spectroscopic imprints on the light emitted by background QSOs. These absorbers are identified as damped Lyα absorption systems. Previous studies of the evolution of the neutral gas (Wolfe et al. 1986, 1995, latter hereafter WLFC95; Lanzetta et al. 1991; Storrie-Lombardi, McMahon, & Irwin 1996b, hereafter SMI96), their metal abundances (Lu et al. 1996; Pettini et al. 1997; Prochaska & Wolfe 1999), their dust content (Fall & Pei 1993; Pei & Fall 1995; Pei, Fall, & Hauser 1999), and their kinematics (Prochaska & Wolfe 1997, 1998a, 1998b) provide compelling evidence that damped absorbers are the progenitors of present-day galaxies. However, substantial debate continues over exactly which galaxies these are (e.g., Le Brun et al. 1997; Haehnelt, Steinmetz, & Rauch 1998; Pettini et al. 1999; Prochaska & Wolfe 1998a, 1998b; Rao & Turnshek 1998; Salucci & Persic 1999). We present results of a new survey for damped Lyα absorbers in the redshift range $z \approx 3$–4.5.

[1] Some of the observations presented here were obtained at the W. M. Keck Observatory, which is operated as a scientific partnership among the California Institute of Technology, the University of California, and the National Aeronautics and Space Administration. The Observatory was made possible by the generous financial support of the W. M. Keck Foundation. Observations were also made using the 3.9 m Anglo-Australian Telescope at the Anglo-Australian Observatory and the Shane 3 m Telescope at the Lick Observatory.

The comoving mass density of neutral gas, $\Omega_g(z)$, at $z \approx 3$ has been known for some time to be comparable to the density of visible matter, i.e., stars in present-day galaxies for an $\Omega = 1$ ($\Lambda = 0$) universe (Rao & Briggs 1993; WLFC95; SMI96). We have improved our estimates of $\Omega_g(z)$ at high redshift with new surveys (this work; Storrie-Lombardi & Hook 2000), and estimates of Ω_* have also been updated (Fukugita, Hogan, & Peebles 1998). The first damped Lyα survey to have a substantial data set with redshifts $z > 3.0$ (Storrie-Lombardi et al. 1996, hereafter SMIH96) hinted at a turnover in $\Omega_g(z)$ at redshifts $z > 4$ (SMI96), prior to which damped Lyα alpha systems might still be collapsing. In this paper we update the discussion of these issues with a larger high-redshift data set.

All the follow-up observations of known candidate damped Lyα absorbers were carried out with the Low-Resolution Imaging Spectrometer (LRIS; Oke et al. 1995) on the Keck 1 telescope. The signal-to-noise ratios of the resulting spectra are $\approx 25{:}1$ per pixel, and the resolution is ≈ 2 Å, thus assuring that the spectra are adequate for testing the damping hypothesis (cf. WLFC95). The survey for new damped Lyα candidates was carried out with LRIS on Keck, the KAST spectrograph at the Lick 120″, and the RGO spectrograph at the Anglo-Australian Telescope.

The paper is organized as follows. In § 2 we present the spectra along with fits of Voigt profiles to the damped Lyα lines to accurately determine the column densities. Section 3 contains a compilation of a statistical sample of damped Lyα systems including results from all available previous surveys. In § 4 we present analyses of the three statistical quantities characterizing the evolution of the damped systems, namely, the number of systems per unit redshift interval, dn/dz, the comoving mass density of neutral gas in units of the current critical density, $\Omega_g(z)$, and the frequency distribution of H I column densities, $f(N, z)$. We discuss our results in § 5.

2. DATA

In this section we first present follow-up spectra of previously reported damped Lyα candidates and then discuss new candidates discovered in our survey.

2.1. *LRIS Spectroscopy*

Table 1 is a journal of observations describing the LRIS observations of 30 QSOs. Column (1) gives the QSO coordinate name, column (2) the emission redshift, column (3) the UT date of the observations, columns (4) and (5) the V and/or R magnitude of the QSO, column (6) the central wavelength of the grating setting, column (7) the exposure time, column (8) the number of grooves per millimeter of the grating, and column (9) a reference to observations reporting discovery of the candidate. The spectra were wavelength-calibrated with a ThAr lamp, flat-fielded with a quartz lamp, and reduced in the usual manner.

2.1.1. *Objects Selected for the Presence of Damped Lyα Candidates*

Table 2 presents results for the subset of 11 QSOs selected for the presence of damped Lyα candidates. We include only those candidates found in surveys specifically designed to search for strong absorption features blueward of Lyα emission. The confirmed damped Lyα systems are thus included in our statistical sample discussed in § 4, which covers lines of sight observed with sufficient accuracy that damped absorption lines arising in gas with $N_{\rm H\,I}$ above the threshold, 2×10^{20} atoms cm^{-2}, could have been detected at the 5 σ confidence level. Column (1) of Table 2 gives the QSO coordinate name, column (2) the emission redshift, columns (3) and (4) the V or R magnitude of the QSO, and columns (5)–(8) the reference for the low-resolution survey that identified the candidate absorber, the absorption redshift, the Lyα equivalent width, and the inferred log N(H I). Columns (9) and (10) give the absorption redshift and log N(H I) deduced by profile fitting from the higher resolution LRIS spectra.

Figure 1 exhibits damped Lyα absorption spectra for the 10 confirmed damped Lyα systems with log $N_{\rm H\,I} \geq 20.3$ cm^{-2} and the $z = 2.8228$ system toward Q0249−2212 in which log $N_{\rm H\,I} = 20.20$ cm^{-2}. Three Voigt profile fits are shown in order of increasing $N_{\rm H\,I}$, with the middle value representing the mean $N_{\rm H\,I}$ inferred from the optimal fit, and the other two judged to be ± 1 σ from the mean. The results of the fits are given in Table 2.

Because the high-density Lyα forest in this redshift range can lead to ambiguities in the fitting procedure, we did a number of simulations creating spectra with damped absorbers in the forest at known redshifts and column densities, and testing our fitting techniques on these prior to making the final fits on the object spectra. These are extensions of the simulations discussed in SMIH96, where the original damped candidates were selected. The continua of the spectra were first fitted with an automated task using cubic splines. These were then modified interactively in dense forest regions, where the continuum was placed too low, i.e., the fit had dipped into the line. In every case, the redshift of the fit is fixed by the low-ion metal lines detected redward of Lyα emission; i.e., outside the Lyα forest, and a χ^2 minimization technique, *vpgti*,[2] is subsequently used to make the fit.

The metal lines were taken from the LRIS spectra when we had wavelength coverage that went far enough into the red to include them. In the other cases we used the metal-line redshifts determined from 5 Å resolution spectra (SMIH96) taken with the ISIS spectrograph on the William Herschel Telescope (WHT). We confirmed that the wavelength calibrations for the WHT and LRIS data agree well in QSOs with overlap regions. The maximum difference in the redshift we determined from the same line measured in different spectra is 0.002, so we are confident that the metal lines in the WHT spectra do not introduce any significant error when applying the measured redshift to the LRIS spectra.

As expected, the higher resolution of the LRIS spectra make the fitting less ambiguous than the candidate-selection process, although the agreement between the estimated and actual column density is very good in almost all cases. It was crucial to have a low-ionization metal line to anchor the redshift for the H I absorption, and in all cases one or both wings of the damped feature provided a good constraint on the column density measurement. Weaker H I components were also used to help constrain the fits, but only the final damped components are shown in the figures.

The following are brief comments on the individual fits:

1. BR B0019−1522: $z_{\rm abs} = 3.4370$, log $N_{\rm H\,I} = 20.92$.—Si II 1527, Fe II 1608, and Al II 1670 were used to determine the redshift. This is the only damped system in which the

[2] Written by R. F. Carswell, J. K. Webb, A. J. Cooke, and M. J. Irwin.

TABLE 1

LRIS JOURNAL OF OBSERVATIONS

QSO (1)	z_{em} (2)	Date (3)	V (4)	R (5)	$\lambda_{central}$ (Å) (6)	Exposure (s) (7)	Grating (g mm^{-1}) (8)	Reference (9)
BR BB0019−1522.....	4.528	1995 Sep 18		19.0	5865	3300	1200	1
					7065	1200	1200	
					7765	1500	1200	
Q0046−293	4.014	1995 Sep 19	19.4		5390	2400	1200	2
					6565	1200	1200	
Q0057−274	3.52	1995 Sep 20		18.73	5085	1500	1200	2
					6260	600	1200	
PSS J0059+0003	4.16	1995 Sep 19		19.5	5190	2400	1200	3
					6365	1200	1200	
PC 0104+0215	4.171	1995 Sep 20	19.7		5390	3600	1200	4
					6565	2400	1200	
BRI B0111−2819	4.30	1995 Sep 20		18.7	5390	4300	1200	5
		1995 Sep 20			6865	1200	1200	
		1995 Sep 19			5190	2400	1200	
		1995 Sep 19			6365	1200	1200	
PC 0131+0120	3.792	1995 Sep 20		19.4	5665	1500	1200	6
					6865	1200	1200	
Q0201+1120.....	3.61	1995 Sep 20	20.1		6500	1600	300	7
		1995 Sep 19			5665	1800	1200	
		1995 Sep 19			6565	1500	1200	
		1995 Sep 19			7565	1200	1200	
PSS J0248+1802	4.43	1995 Sep 18		18.4	5190	1700	1200	3
					6365	1200	1200	
					7565	600	1200	
Q0249−222	3.20	1995 Sep 18	18.4		5190	1200	1200	8
					6365	500	1200	
PC 0345+0130	3.638	1995 Sep 20	19.9		5190	2400	1200	6
		1995 Sep 19			6260	1500	1200	
PC 0751+5622	4.281	1995 Mar 7	19.7		6150	3600	1200	4
BR B0951−0450	4.369	1995 Mar 7		18.9	6150	2800	1200	1
BRI B0952−0115	4.426	1995 Mar 7		18.7	6150	2200	1200	1
PC 0953+4749	4.46	1995 Mar 7	19.3		5450	5400	1200	9
BRI B1013+0035	4.405	1995 Mar 7		18.8	5450	3200	1200	1
BRI B1114−0822	4.495	1995 Mar 7		19.4	6150	3600	1200	1
PSS J1317+3531	4.365	1996 May 16		19.1	6500	622	300	3
BRI B1346−0322	3.992	1995 Mar 7		19.1	6150	2800	1200	1
PSS J1430+2828	4.306	1996 May 16		19.3	6500	600	300	3
PSS J1435+3057	4.297	1996 May 16		19.3	6500	600	300	3
PSS J1443+2724	4.407	1996 May 16		19.3	6500	600	300	3
MG 1500+0431	3.67	1995 Sep 20		18.01	5085	1200	1200	10
					6260	600	1200	
BRI B1500+0824	3.943	1995 Mar 7		19.3	5100	1800	1200	1
PC 1548+4637	3.544	1995 Sep 20	19.2		5085	2400	1200	9
					6260	600	1200	
PC 1640+4628	3.700	1995 Sep 19	19.5		5085	1800	1200	9
		1995 Sep 20			6260	2100	1200	
PC 2047+0123	3.799	1995 Sep 18	19.7		5085	5400	1200	9
					6260	1800	1200	
Q2050−359	3.49	1995 Sep 19	18.3		5085	1200	1200	2
					6260	600	1200	
BR B2237−0607	4.558	1995 Sep 18		18.3	6565	2400	1200	1
					7765	1200	1200	
PC 2331+0216	4.093	1995 Sep 19	20.0		5665	2800	1200	4
					6865	1200	1200	

REFERENCES.—(1) SIM96; (2) Warren et al. 1991; (3) Kennefick et al. 1995; (4) Schneider et al. 1989; (5) McMahon & Irwin 1995, private communication; (6) Schneider et al. 1987; (7) White et al. 1993; (8) Sargent et al. 1989; (9) Schneider et al. 1991; (10) McMahon et al. 1994.

TABLE 2

LRIS FOLLOW-UP OF CANDIDATE DAMPED Lyα ABSORBERS

	QSO PROPERTIES			SURVEY DATA				FOLLOW-UP PROPERTIES	
QSO (1)	z_{em} (2)	V (3)	R (4)	Reference (5)	z_{abs} (6)	W (Å) (7)	log $N_{H\,I}$ (cm^{-2}) (8)	z_{abs} (9)	log $N_{H\,I}$ (cm^{-2}) (10)
BR B0019−1522.....	4.528		19.0	1	3.42	7.6	20.0	3.4370	20.92 ± 0.10
				1	3.98	12.3	20.5	not damped	
				1	4.28	8.0	20.1	not damped	
BRI B0111−2819.....	4.30		18.7	2	3.100	23.4	21.0	3.1043	21.0 ± 0.1
Q0249−2212.....	3.202	18.4		3	2.831	10.2	...	2.8228	20.2 ± 0.1
BR B0951−0450.....	4.369		18.9	1	3.84	24.0	21.0	3.8477	20.6 ± 0.1
				1	4.20	10.6	20.3	4.2028	20.4 ± 0.1
BRI B0952−0115.....	4.426		18.7	1	4.01	18.0	20.8	4.0221[a]	20.2
								4.0255[b]	20.3
								4.0238[c]	20.55 ± 0.10
BRI B1013+0035.....	4.405		18.8	1	3.10	17.5	20.8	3.1031	21.1 ± 0.1
				1	3.73	9.6	20.2	not damped	
BRI B1114−0822.....	4.495		19.4	1	3.91	6.7	19.9	not damped	
				1	4.25	11.7	20.4	4.2576	20.3 ± 0.1
				1	4.45	5.3	19.7	not damped	
BRI B1346−0322.....	3.992		19.1	1	3.73	10.0	20.3	3.7343	20.72 ± 0.10
BRI B1500+0824.....	3.943		19.3	1	2.80	11.3	20.4	2.7968	20.8 ± 0.2
BR B2237−0607.....	4.558		18.3	1	4.08	11.5	20.4	4.0683[a]	20.2
								4.0699[b]	20.25
								4.0691[c]	20.5 ± 0.1

[a] Component *a*.
[b] Component *b*.
[c] Components *a* and *b* combined.
REFERENCES.—(1) SIM96; (2) this paper; (3) Sargent et al. 1989.

column density estimated from the 5 Å resolution WHT spectrum was substantially in error. This is due to the fact that it lies at 5400 Å, which is precisely where the blue and red arms of the ISIS spectra were pasted together.

2. BRI B0111−2819: $z_{abs} = 3.1043$, log $N_{H\,I} = 21.0$.—Si II 1808 was used to determine the redshift. We did not use the Fe II 1608 and Al II 1670 transitions because they were very broad. We also fitted a weaker component with $z = 3.070$ and log $N_{H\,I} = 19.5$ cm^{-2}.

3. Q0249−2212: $z_{abs} = 2.8228$, log $N_{H\,I} = 20.2$.—Al II 1670 was used to fix the redshift. The fit is excellent, owing to absence of Lyα forest confusion noise near the center of the line profile. Note that the fitted column density, log $N_{H\,I} = 20.2$ cm^{-2}, removes this object from the statistical sample.

4. BR B0951−0450: $z_{abs} = 3.8580$, log $N_{H\,I} = 20.6$.—In common with many other damped Lyα systems observed at $z > 3$, substantial Lyα forest structure interferes with the fitting procedure in the wings of the damped feature. In this case we used Si II 1527 observed at low resolution (FWHM = 5 Å) with the WHT to anchor the redshift. The column density is constrained by the bump at 5875 Å and the wings on both sides.

5. BR B0951−0450: $z_{abs} = 4.2028$, log $N_{H\,I} = 20.4$.—We again used Si II 1527 from the WHT spectrum to determine the redshift. The fit is very good, due to the lack of Lyα forest confusion near the line center.

6. BRI B0952−0115: $z_{abs} = 4.0238$, log $N_{H\,I} = 20.55$.—A strong C II 1334 line from the LRIS spectrum anchors the fit. The figure shows that the fit is somewhat uncertain, owing to strong Lyα absorption in the blue wing of the damped profile. However, the resulting log $N_{H\,I}$ is well determined because the red wing and the blue positive feature near 6085 Å place strong constraints on the fit.

7. BRI B1013+0035: $z_{abs} = 3.1031$, log $N_{H\,I} = 21.1$.—We used metal lines from the WHT spectrum to fix the redshift, because our limited coverage with LRIS placed all the strong low-ion metal transitions in the Lyα forest. The Lyα forest confusion is especially strong in the blue wing of the damping profile. Nevertheless, the fit is again constrained by the observed red wing of the profile and the positive spikes blueward of the profile.

8. BRI B1114−0922: $z_{abs} = 4.2576$, log $N_{H\,I} = 20.3$.—There is no LRIS coverage redward of Lyα emission, so we again used metal lines from the WHT spectrum. However, the fit was well constrained by statistically significant positive spikes on both the red and blue wings of the damping profile.

9. BRI B1346−0322: $z_{abs} = 3.7343$, log $N_{H\,I} = 20.72$.—This damping profile is the best determined of this sample because the redshift is fixed by a single strong C II line in the LRIS spectrum. In addition, the absence of significant Lyα forest absorption in the profile wings results in an excellent fit.

10. BRI B1500+0824: $z_{abs} = 2.7968$, log $N_{H\,I} = 20.8$.—Because of limited integration time, this is the noisiest spectrum we obtained. However, the rise of the spectrum to the red of the damped Lyα trough places an upper limit not far above the quoted value for $N_{H\,I}$. The greater uncertainties are reflected in the larger error bars of the fit. We used WHT metal lines to anchor the redshift, because of our limited LRIS coverage.

11. BR B2237−0607: $z_{abs} = 4.0691$, log $N_{H\,I} = 20.5$.—In this case we used C II 1334, which had two strong absorp-

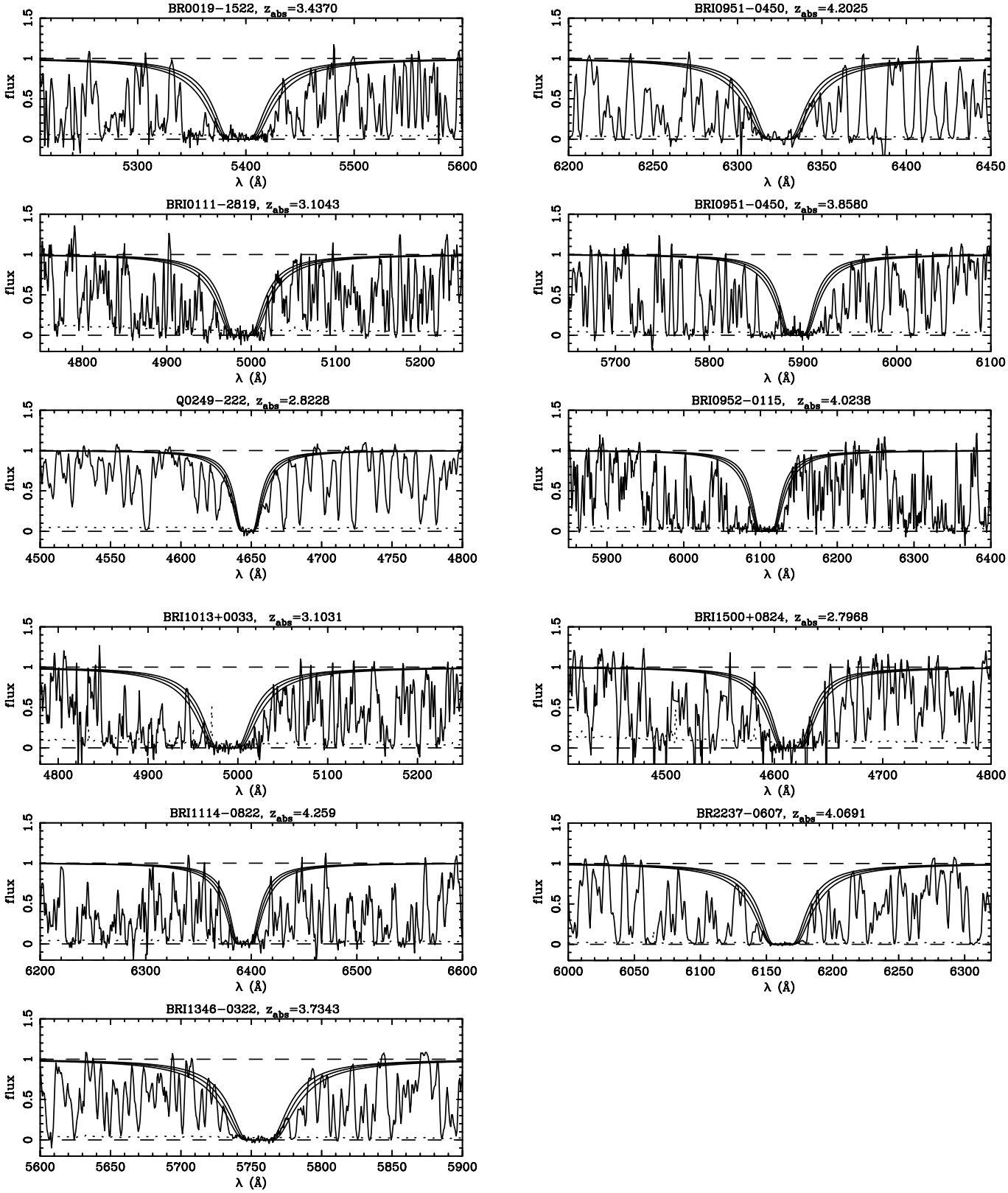

FIG. 1.—Spectra for the 10 confirmed damped Lyα systems with $\log N_{\rm H\,I} \geq 20.3$ cm^{-2} and the $z = 2.8228$ system toward Q0249−2212 in which $\log N_{\rm H\,I} = 20.20$ cm^{-2}. Three Voigt profile fits are shown in order of increasing $N_{\rm H\,I}$, with the middle value representing the mean $N_{\rm H\,I}$ inferred from the optimal fit, and the other two judged to be $\pm 1\,\sigma$ from the mean. The results are summarized in Table 2.

tion components. Both were used to form the fit shown in Figure 1. It is well constrained, owing to the high signal-to-noise ratio of the data. This object has since been observed with HIRES (Lu et al. 1996), and their result agrees well with ours (log $N_{\rm H\,I} = 20.5$).

2.1.2. *New LRIS Survey for Damped Lyα Systems*

We obtained LRIS spectra for 19 high-redshift QSOs that had not been previously studied for the presence of damped Lyα lines and one QSO with a known damped absorber (Q0201+1120). The objects not previously surveyed come from several quasar samples (Warren, Hewett, & Osmer 1991; Schneider, Schmidt, & Gunn 1987, 1989, 1991; McMahon et al. 1994; Kennefick et al. 1995). Because these objects were not selected on the basis of absorption properties, their spectra are included in constructing the selection function, $g(z)$, which describes the redshift sensitivity of the survey. The survey details are listed in Table 3. In cases in which damped Lyα lines are detected, the spectra are used for fitting Voigt profiles, as in § 2.1.1. We show the spectra for all 20 QSOs in Figure 2, since even intermediate-quality data are lacking for most of these objects. The 1 σ error arrays are overplotted, although these are difficult to see in most cases because the signal-to-noise ratio is ≥ 25. In Figure 3 we show the spectra for the confirmed damped systems. The damped candidate and confirmed absorbers are discussed individually below.

1. Q0046−293: $z_{\rm abs} = 3.0589$, log $N_{\rm H\,I} = 20.1$.—The redshift was determined from narrow Si II 1526, Fe II 1608, and Al II 1670, and the fit is well constrained by the steep sides of the H I trough. This system is not included in the statistical sample, since as it falls below the threshold of log $N_{\rm H\,I} = 20.3\ {\rm cm}^{-2}$.

2. Q0046−293: $z_{\rm abs} = 3.841$, log $N_{\rm H\,I} = 20.1$.—This system is composed of two components, with the redshifts determined from C II 1334. It is also well constrained by the H I line. This system is not included in the statistical sample, since it falls below the threshold of log $N_{\rm H\,I} = 20.3\ {\rm cm}^{-2}$.

3. Q0057−274: $z_{\rm abs} = 3.2413$, log $N_{\rm H\,I} = 19.8$.—The redshift was determined from C II 1334, and the fit is well constrained by the sides of the H I trough. This system is not included in the statistical sample, since it falls below the threshold of log $N_{\rm H\,I} = 20.3\ {\rm cm}^{-2}$.

4. PSS J0059+0003: $z_{\rm abs} = 3.1043$, log $N_{\rm H\,I} = 20.0$.—The redshift is well determined from Si II 1526. Although there is strong Lyα absorption in the blue wing of the damped profile, the resulting log $N_{\rm H\,I}$ is accurate because the red wing places a strong constraint on the fit.

TABLE 3

NEW LRIS SURVEY DATA

QSO	$z_{\rm em}$	$z_{\rm min}$	$z_{\rm max}$	$z_{\rm abs}$	W (Å)	log $N_{\rm H\,I}$ (cm^{-2})
Q0046−293.....	4.014	2.882	3.964	3.0589		20.1 ± 0.1
				3.8407[a]		19.9 ± 0.1[a]
				3.8422[b]		19.6 ± 0.1[b]
				3.841[c]		20.1 ± 0.1[c]
Q0057−274.....	3.52	2.603	3.475	3.2413		19.8 ± 0.1
PSS J0059+0003.....	4.16	2.750	4.108	3.1043		20.0 ± 0.1
PC 0104+0215.....	4.171	2.881	4.119			
PC 0131+0120.....	3.792	3.116	3.744			
Q0201+1120	3.61	...	...	3.3848		21.3 ± 0.1
PSS J0248+1802.....	4.43	2.810	4.376			
PC 0345+0130.....	3.638	2.699	3.592			
PC 0751+5623.....	4.281	3.526	4.228			
PC 0953+4749.....	4.457	3.010	4.004	3.403		≤ 20.9
				3.890		≤ 21.1
PSS J1317+3531.....	4.365[d]	2.978	4.311			
PSS J1430+2828.....	4.306[d]	2.777	4.253			
PSS J1435+3057.....	4.297[d]	2.905	4.244	3.26	7.6	20.0
				3.51	7.5	20.0
				3.71	7.3	20.0
PSS J1443+2724.....	4.407[d]	2.950	4.353	4.216	18.1	20.8
MG 1500+0431.....	3.67	2.606	3.623			
PC 1548+4637.....	3.544	2.607	3.499			
PC 1640+4628.....	3.700	2.604	3.653			
PC 2047+0123.....	3.799	2.620	3.751	2.7299	11.2	20.4 ± 0.1
Q2050−359.....	3.49	2.605	3.445	2.98	7.8	not damped
PC 2331+0216.....	4.093	3.115	4.042			

NOTE.—Confirmed systems have uncertainties quoted for the column density measurements. The candidate systems do not. Previous experience shows that the system in PSS J1443+2724 is highly likely to be damped, and the candidates in PSS J1435+3057 are highly unlikely to be damped. All the candidate and confirmed systems with log $N_{\rm H\,I} \geq 20.3$ are included in the statistical sample in the analysis that follows, expect for Q0201+1120. It was observed because of a known damped absorber, not in an unbiased survey.

[a] Component *a*.

[b] Component *b*.

[c] Components *a* and *b* combined.

[d] Emission redshifts for these QSOs have been determined from the mean redshifts of the O I 1302, Si IV + O IV 1400, and C IV 1549 emission lines observed in the LRIS spectra.

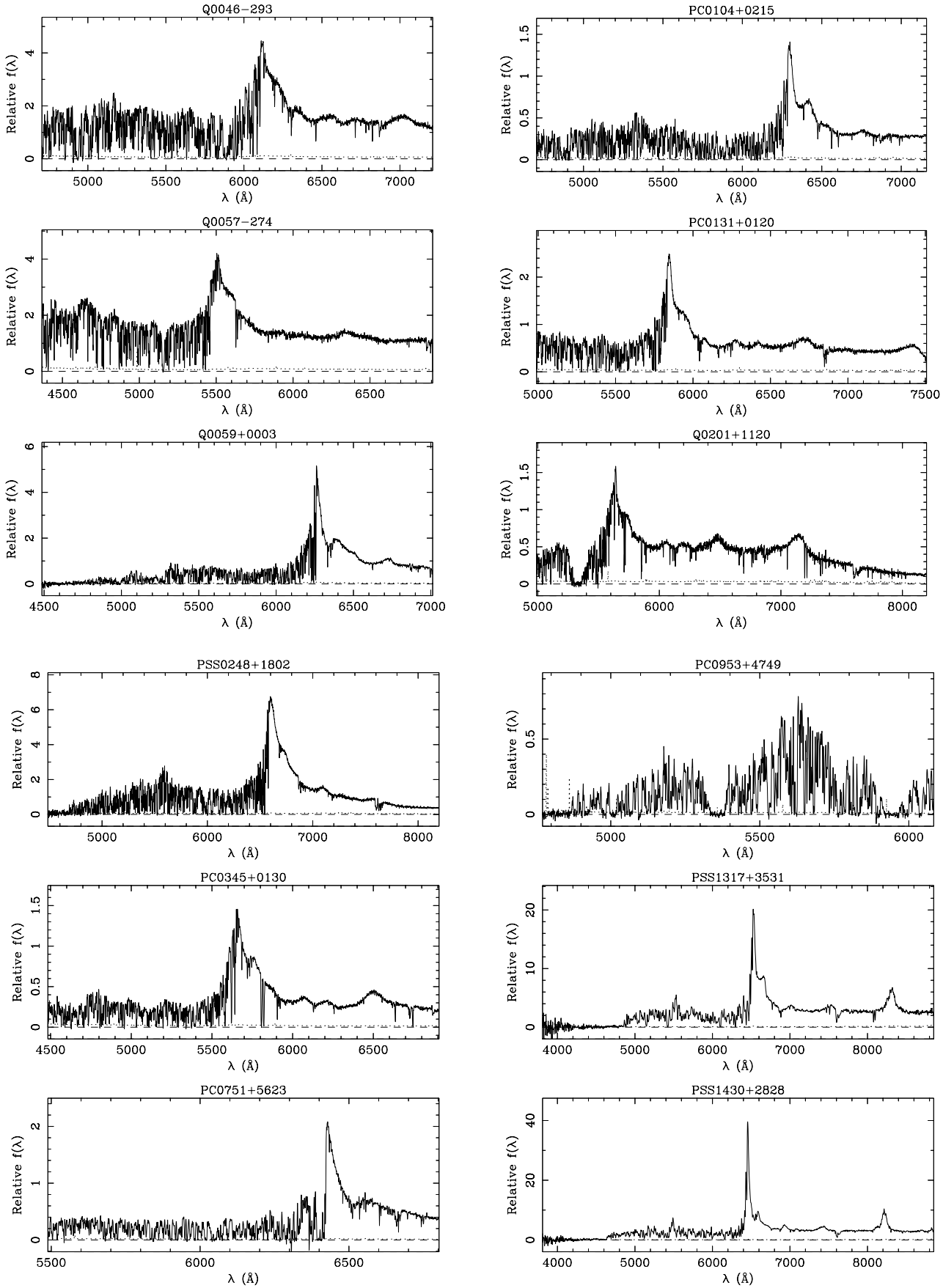

FIG. 2.—All the spectra taken in the new LRIS survey, plus Q0201 + 1120. The 1 σ error arrays are overplotted as dashed lines, although these are difficult to see in most cases due to the high signal-to-noise ratios of the spectra. The observations are summarized in Table 3. Expanded versions of the region around the confirmed damped systems are shown in Fig. 3.

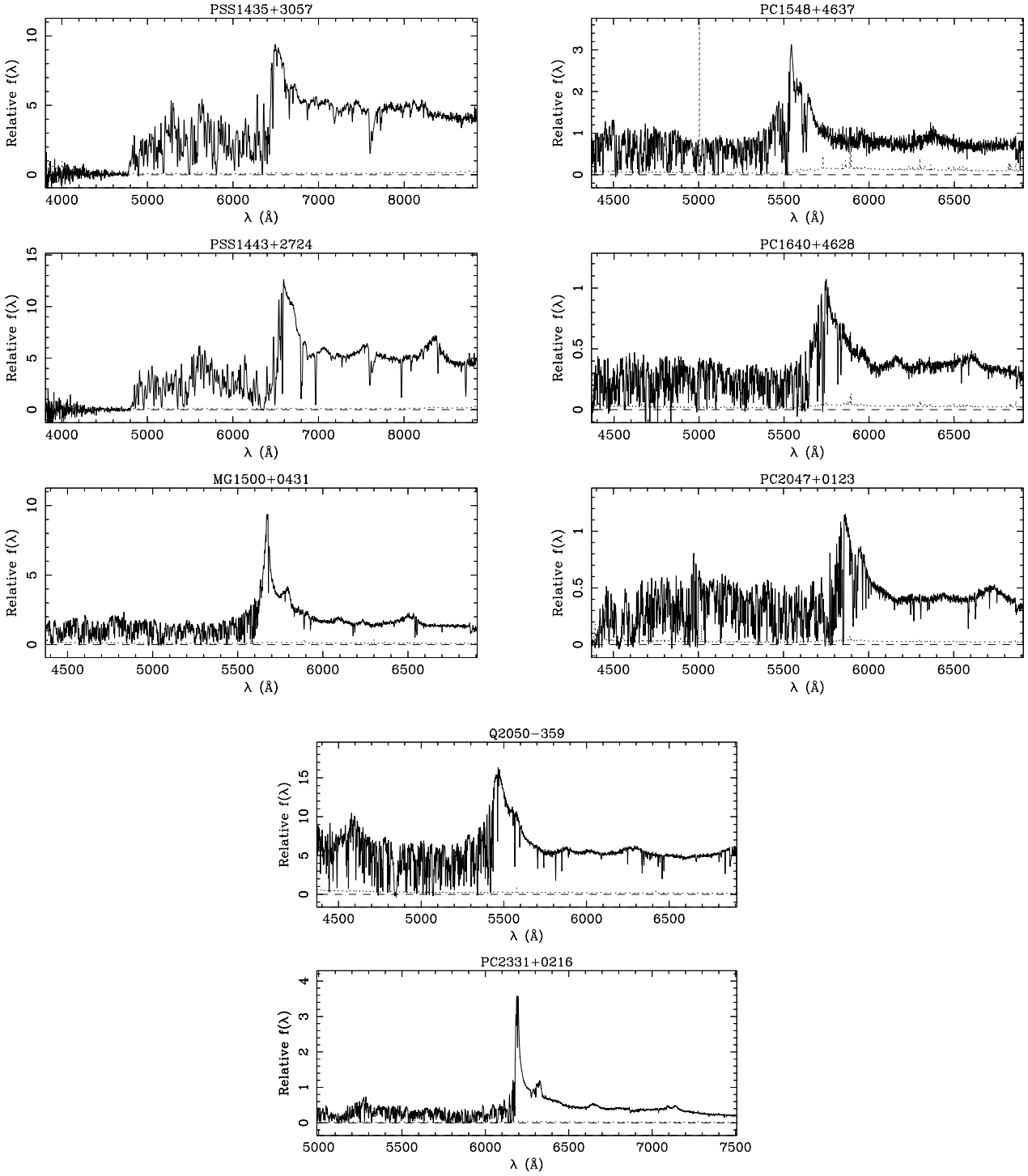

FIG. 2.—*Continued*

5. Q0201+1120: $z_{\rm abs} = 3.3848$, $\log N_{\rm H\,I} = 21.3$.—The damped system in this QSO was studied by White, Kinney, & Becker (1993) in a spectrum with ≈ 10 Å resolution. We have wavelength coverage from 5000−8000 Å, which includes several low-ionization metal lines from the damped absorber. Our column density and redshift measurements are in excellent agreement with those previously published.

6. PC 0953+4749: $z_{\rm abs} = 3.403$, $\log N_{\rm H\,I} \leq 20.9$; $z_{\rm abs} = 3.890$, $\log N_{\rm H\,I} \leq 21.1$.—We originally observed this object because of the obvious large absorption features visible in the published spectrum. We did not plan to include it in the statistical sample because (1) the QSO was approximately a magnitude fainter than the objects we were originally following up, and (2) we observed it because we knew it might have high column damped features. When we completed our new survey, we had observed and included in our statistical sample all the QSOs with $V \leq 19.5$ and $z \geq 3.5$ that were available at the time. This object has a published V magnitude of 19.5, so we now include it in our statistical

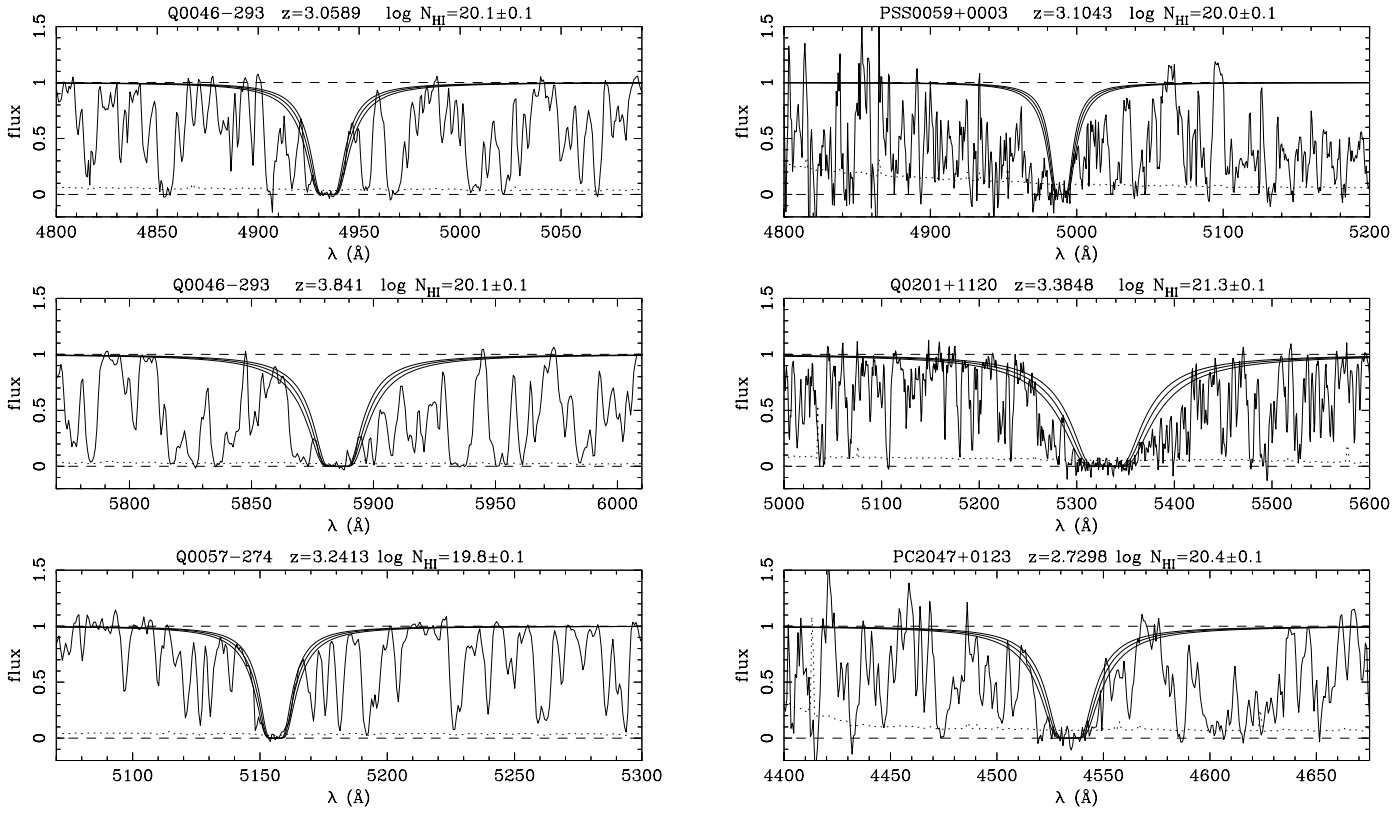

FIG. 3.—Confirmed damped Lyα systems with log $N_{\rm H\,I} \geq 20.3$ cm^{-2} from the new survey. Three Voigt profile fits are shown in order of increasing $N_{\rm H\,I}$, with the middle value representing the mean $N_{\rm H\,I}$ inferred from the optimal fit, and the other two judged to be $\pm 1\ \sigma$ from the mean. The results are summarized in Table 3.

sample. It is problematic, since it is one of the faintest objects we observed and we only have wavelength coverage at one blue setting. The existing QSO spectra have 25 Å resolution, which is too low to provide any useful metal-line information. Even though the 1.5 Å resolution LRIS spectrum has a sufficient signal-to-noise ratio to fit the H I, we are unable to accurately anchor the redshifts for these absorbers, so the column densities quoted are upper limits.

7. PSS J1435+3057: $z_{\rm abs} = 3.26$, log $N_{\rm H\,I} = 20.0$; $z_{\rm abs} = 3.51$, log $N_{\rm H\,I} = 20.0$; $z_{\rm abs} = 3.71$, log $N_{\rm H\,I} = 20.0$.—Previous experience shows that these candidates are highly unlikely to be damped. They are not included in the statistical sample in the analysis that follows.

8. PSS J1443+2724: $z_{\rm abs} = 4.216$, log $N_{\rm H\,I} = 20.8$.—Although taken with the 300 g mm^{-1} grating, the signal-to-noise ratio in this spectrum is high enough to determine that this absorber is highly likely to be damped. The redshift was determined from the strong, narrow C II 1334 line.

9. PC 2047+0123: $z_{\rm abs} = 2.7299$, log $N_{\rm H\,I} = 20.4$.—Although the only useful low-ion metal lines, C II 1334 and Fe II 1608, were in the Lyα forest portion of the LRIS spectrum, we believe that the redshift is well determined, since neither metal line was severely blended.

10. Q2050+359: not damped.—Although the feature at ≈4843 Å appears to be damped at first glance, an examination of the associated metal lines reveals that it is not. There is a complex of low- and high-ionization metals lines that cover the redshift range $2.98 \leq z \leq 3.17$, and there is no suitable fit for a damped Lyα feature with log $N_{\rm H\,I} \geq 20.0$. It is a complex of lower column density lines.

2.1.3. *New Lick/AAT Survey for Damped Lyα Systems*

Ten additional QSOs with redshifts $z \geq 4$ were observed at the Lick 3 m telescope with the KAST spectrograph or the Anglo-Australian Telescope with the RGO spectrograph, at ≈6 Å resolution. The survey data from these objects are summarized in Table 4, and the spectra are shown in Figure 4. PSS J0244−0108 is excluded from further analysis because it exhibits broad absorption lines believed to be intrinsic to the quasar. Four damped candidates were detected in these spectra, and their estimated column densities were determined from the measured equivalent widths of the lines. This method is discussed in detail in Lanzetta et al. (1991), and its application to $z > 4$ QSOs is discussed in SMIH96. BRI B0111−2819 was subsequently followed up with LRIS and is included in Table 2.

3. STATISTICAL SAMPLE

The statistical sample of damped absorbers includes all confirmed or candidate damped Lyα absorbers with neutral hydrogen column densities $N_{\rm H\,I} \geq 2 \times 10^{20}$ atoms cm^{-2} from surveys designed to detect these absorbers (Wolfe et al. 1986; Lanzetta et al. 1991; Lanzetta, Wolfe, & Turshek 1995, hereafter LWT95; WLFC95; SMIH96; Storrie-Lombardi, Irwin, & McMahon 1996a, hereafter SIM96; Storrie-Lombardi & Hook 2000; this paper). The QSOs with damped absorbers are listed in Table 5. The QSO spectra that did not contain damped absorbers, and the redshift path they contribute, are listed in Table 6. This includes 646 QSO lines of sight and 85 damped Lyα

TABLE 4

NEW LICK/AAT SURVEY DATA

QSO	Reference	R	Observation	Date	Exposure (s)	z_{em}	z_{min}	z_{max}	z_{abs}	W (Å)	log $N_{H\,I}$ (cm^{-2})
PSS J0030+1702.....	1	19.3	Lick	1995 Oct 24	10800	4.282	2.763	4.229			
BRI B0046−2458	2	18.9	AAT	1995 Aug 27	3600	4.15	2.575	4.099			
BRI B0111−2819	2	18.7	AAT	1995 Aug 27	3295	4.30	2.908	4.247	3.100	23.4	21.0[a]
PSS J0117+1552.....	1	18.6	Lick	1995 Oct 24	5400	4.244	2.646	4.192			
PSS J0132+1341.....	1	19.3	Lick	1995 Oct 24	7200	4.147	2.844	4.096	3.93	10.5	20.3
BRI B0135−4239	2	18.5	AAT	1995 Aug 27	4200	3.97	2.575	3.920			
PSS J0244−0108[b].....	1	19.0	Lick	1995 Oct 24	3300	4.00					
BR B0331−1622	2	17.9	Lick	1995 Oct 23	9000	4.40	2.868	4.326	3.56	14.6	20.6
PSS J1057+4555.....	1	17.7	Lick	1995 Oct 20, 23	4500	4.101	2.652	4.050	3.05	10.2	20.3
BR B1600+0729	2	18.8	Lick	1996 Mar 16	4200	4.38	3.062	4.326			

NOTE.—The Lick observations were taken at the 120″ with the KAST spectrograph, with simultaneous blue and red arm observations. The Anglo-Australian Telescope observations were taken with the RGO spectrograph. All are at approximately 6 Å resolution (FWHM). For the spectra with enough wavelength coverage to the red to see C IV, the QSO emission redshifts have been determined from a mean of the O I 1302, Si IV + O IV 1400, and C IV 1549 emission lines.

[a] This damped candidate was subsequently observed with LRIS (see Table 2 and Fig. 2).

[b] This QSO exhibits broad absorption lines and is excluded from further consideration.

REFERENCES.—(1) Kennefick et al. 1995 and J. Kennefick 1995, private communication; (2) M. Irwin 1995, private communication

absorbers. The spectra for all of these lines of sight had sufficient signal-to-noise ratio for us to detect damped absorption with $N_{H\,I}$ above the threshold at the 5 σ confidence level between the redshifts z_{min} and z_{max} listed in the tables. The redshift path surveyed in each QSO is used to construct the sensitivity function, $g(z)$. It gives the number of lines of sight at a given redshift over which damped systems can be detected at a greater than 5 σ level. The form of the selection function is given by

$$g(z) = \sum_{i=1}^{m} \Theta(z_i^{max} - z)\Theta(z - z_i^{min}) \quad (1)$$

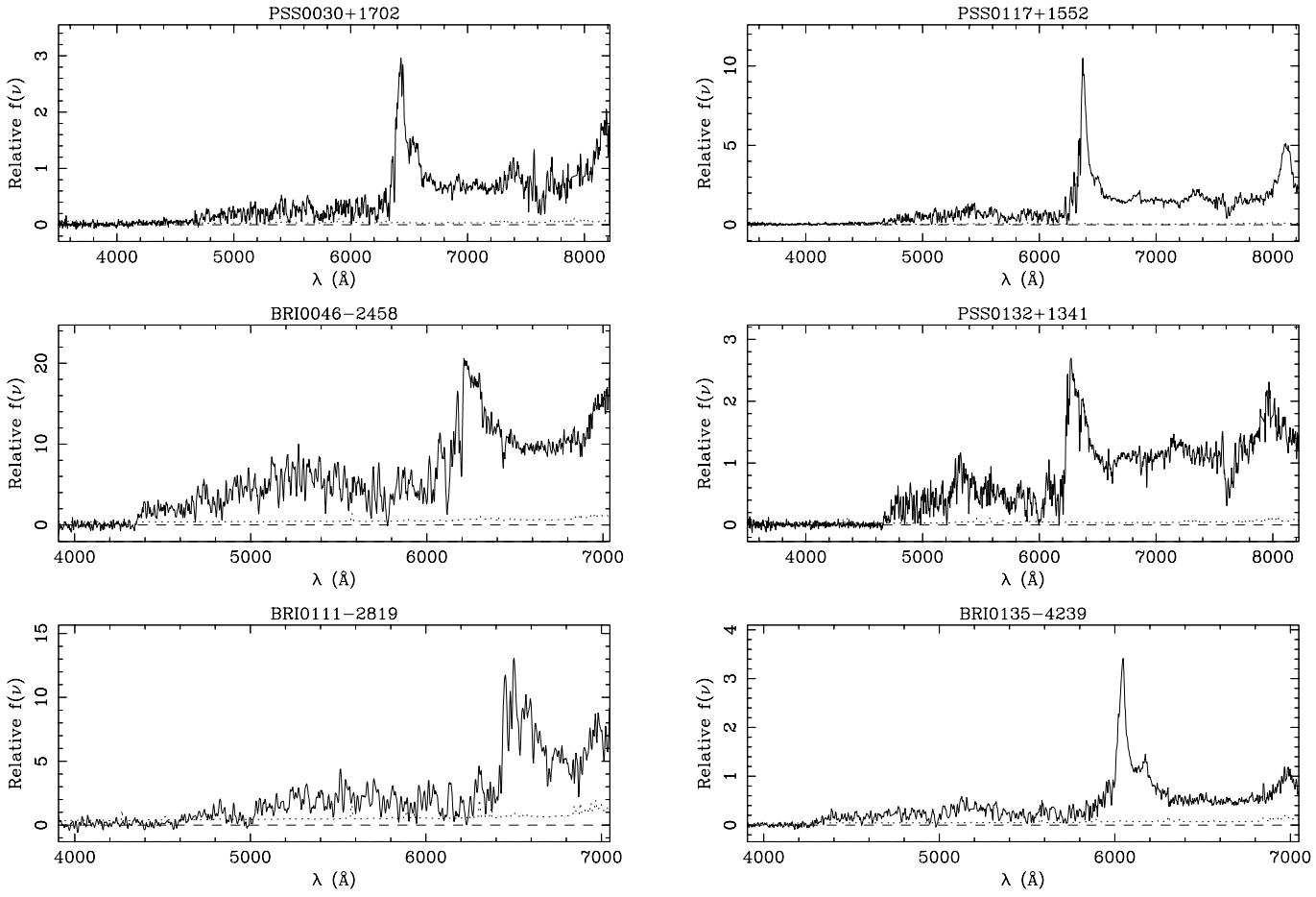

FIG. 4.—Survey spectra taken at the Lick 3 m and the Anglo-Australian Telescope. The data are summarized in Table 4.

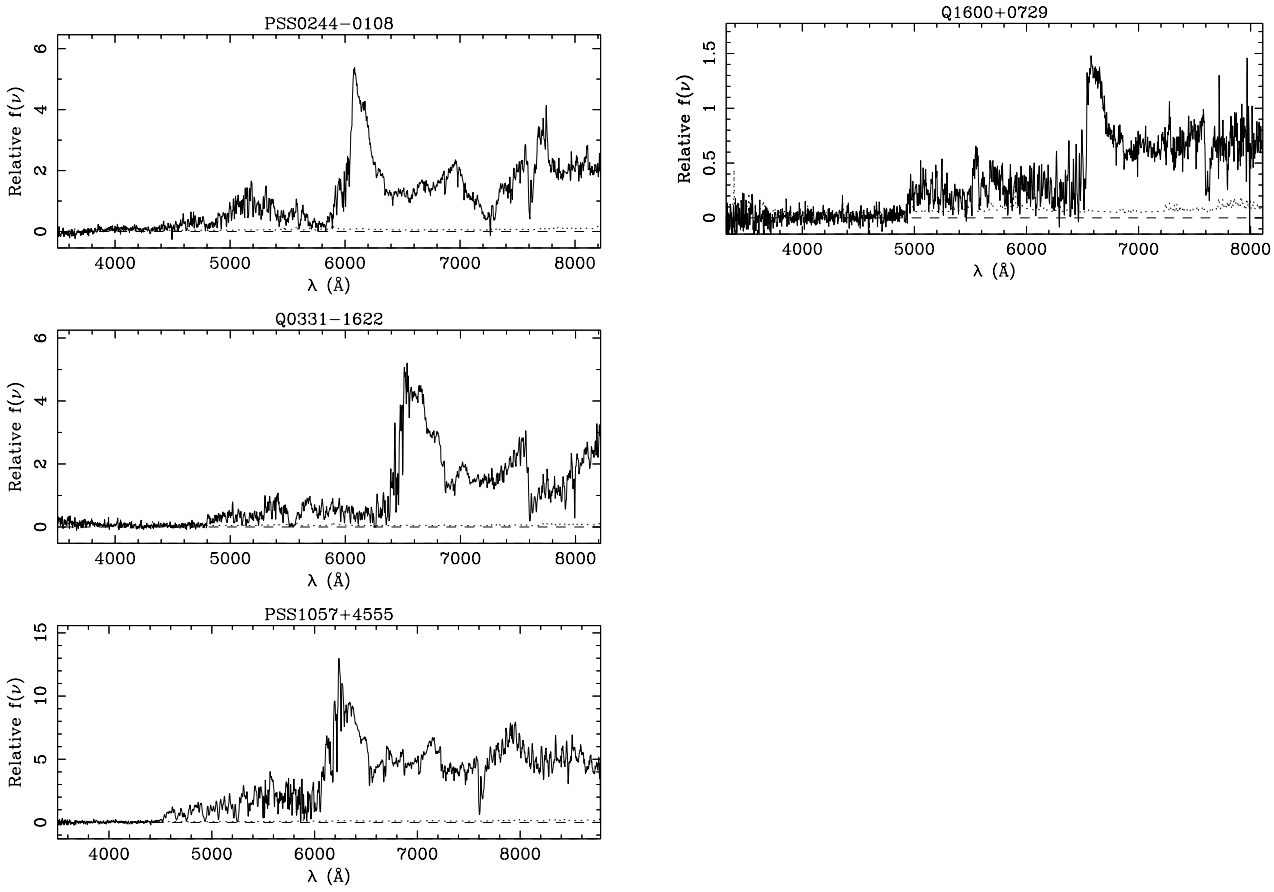

FIG. 4.—*Continued*

TABLE 5

STATISTICAL SAMPLE: QSOs WITH DAMPED Lyα ABSORBERS

QSO	z_{em}	z_{min}	z_{max}	z_{abs}	log $N_{H\,I}$ (cm^{-2})	References
Q0000−2619	4.11	2.389	4.060	3.3901	21.4	1, 2
Q0010−0012	2.15	1.634	2.119	2.0233	20.8	3, 4
Q0013−0029	2.08	1.634	2.049	1.9730	20.7	3, 5
BR B0019−1522.....	4.528	2.97	4.473	3.4370	20.92	6, 7
Q0027+0103	2.29	1.634	2.257	1.9375	20.6	3, 4
Q0042−2930	2.39	1.591	2.354	1.931	20.5[a]	3
Q0049−2820	2.26	1.638	2.223	2.0713	20.5	3, 5
Q0056+0125	3.16	2.197	3.119	2.7750	21.0	3, 4
Q0058−2914	3.07	1.778	3.052	2.6711	21.2	8
Q0100−3105	2.64	1.687	2.605	2.131	20.5[a]	3
Q0100+1300	2.69	1.64	2.74	2.3093	21.4	9, 10
Q0102−1902	3.04	2.044	2.995	2.3693	21.0	1, 13
Q0102−0214	1.98	1.649	1.949	1.7431	20.6	3, 4
BRI B0111−2819.....	4.30	2.709	4.247	3.1043	21.0	7
Q0112−3041	2.99	1.881	2.945	2.4191	20.5	8, 11
	...	...	...	2.7023	20.3	8, 11
Q0112+0300	2.81	1.813	2.785	2.4227	21.0	1, 5
PSS J0132+1341	4.147	2.844	4.096	3.93	20.3	7
Q0149+3335	2.43	1.64	2.43	2.1413	20.5	9, 12
Q0201+3634	2.49	1.632	2.879	2.4614	20.4	8, 13
	...	...	...	1.768	20.5[a]	8
Q0216+0803	3.00	1.731	2.953	2.2930	20.5	1, 11
BR B0331−1622.....	4.38	2.868	4.326	3.56	20.6	7
Q0336−0142	3.20	2.109	3.155	3.0619	21.2	8, 13
Q0347−3819	3.23	2.044	3.186	3.0244	20.8	8, 14
Q0449−1330	3.097	2.006	3.056	2.052	20.4[a]	8
Q0458−0203	2.29	1.96	2.29	2.0399	21.7	9, 12
Q0528−2505	2.779	1.961	2.741	2.1404	21.0	1

TABLE 5—*Continued*

QSO	z_{em}	z_{min}	z_{max}	z_{abs}	log $N_{H\,I}$ (cm^{-2})	References
Q0834−2006	2.75	1.632	2.704	1.715	20.4	8
Q0836+1122	2.70	1.74	2.67	2.4660	20.6	9, 15
Q0913+0715	2.78	1.866	2.739	2.6187	20.3	6, 13
MG 0930+2858	3.41	2.173	3.366	3.24	20.5	16
Q0935+4143	1.9800	1.0626	1.550	1.369	20.3[a]	17
BR B0951−0450.....	4.369	2.93	4.315	3.8580	20.6	6, 7
	...	...	...	4.2028	20.4	6, 7
BRI B0952−0115.....	4.426	2.99	4.372	4.0238	20.55	6, 7
PC 0953+4749	4.457	3.010	4.004	3.403	20.9	7
	...	...	...	3.890	21.1	7
BRI B1013+0035.....	4.405	2.61	4.351	3.1031	21.1	6, 7
Q1032+0414	3.39	2.067	3.347	2.839	20.3[a]	8
PSS J1057+4555	4.101	2.652	4.050	3.05	20.3	7
BRI B1108−0747.....	3.922	2.64	3.873	3.607	20.33	6, 18
BRI B1114−0822.....	4.495	3.19	4.440	4.2576	20.3	6, 7
Q1151+0651	2.76	1.65	2.76	1.7737	21.3	9, 15
Q1159+0132	3.27	1.988	3.226	2.6846	21.1	8, 13
BR B1202−0725.....	4.694	3.16	4.637	4.383	20.49	6, 18
Q1205+0918	2.08	1.634	2.046	1.673	20.6[a]	3
Q1209+0919	3.30	2.175	3.254	2.5835	21.4	8, 13
Q1210+1731	2.54	1.634	2.502	1.8920	20.6	3, 4
Q1215+3322	2.61	1.64	2.60	1.9989	21.0	9, 12
Q1223+1753	2.92	1.945	2.879	2.4658	21.5	3, 5
Q1232+0815	2.57	1.789	2.534	2.3376	20.9	3, 4
Q1240+1516	2.28	1.634	2.247	1.738	20.7[a]	3
Q1244+3443	2.48	1.64	2.50	1.8593	20.5	9, 12
Q1246−0217	2.11	1.634	2.075	1.779	21.2[a]	3
Q1308+0105	2.80	1.634	2.763	1.762	20.6[a]	3
GB 1320+3927	2.98	1.968	2.940	2.11	20.4	16
Q1329+4117	1.9350	0.4853	0.6318	0.5193	20.7[a]	17
Q1337+1121	2.92	1.86	2.92	2.7957	20.9	9, 15
BRI B1346−0322.....	3.992	2.65	3.942	3.7343	20.72	6, 7
Q1347+1116	2.70	1.92	2.71	2.4709	20.3	9, 15
Q1409+0930	2.86	1.979	2.800	2.4561	20.5	8, 13
PSS J1443+2724	4.407	2.950	4.353	4.216	20.8	7
Q1451+1223	3.26	2.158	3.207	2.478	20.4[a]	9, 8
BRI B1500+0824.....	3.943	2.39	3.894	2.7968	20.8	6, 7
GB 1610+2806	3.54	2.021	3.498	2.59	20.6	16
MG 1614+0506	3.21	1.984	3.168	2.52	20.4	16
GB 1759+7539	3.05	1.955	3.010	2.624	20.77	16
PC 2047+0123	3.799	2.620	3.751	2.7299	20.4	7
Q2112+0555	0.4660	0.1105	0.4513	0.2039	20.4[a]	17
Q2132−4321	2.42	1.595	2.386	1.916	20.7[a]	3
Q2138−4427	3.17	2.107	3.128	2.851	20.9	3, 19
Q2206−1958	2.56	1.85	2.58	1.9205	20.5	9, 20
	...	...	...	2.0763	20.7	9, 21
Q2223−0512	1.4040	0.4159	0.6310	0.4925	20.9[a]	17
	...	0.9259	1.3800	...	...	17
Q2230+0232	2.15	1.634	2.119	1.8642	20.8	3, 4, 5
Q2231−0015	3.015	1.749	2.980	2.0657	20.6	3, 11
BR B2237−0607.....	4.558	2.96	4.502	4.0691	20.5	6, 7
Q2239−3836	3.55	2.389	3.508	3.2810	20.8	8, 11
Q2248+0127	2.56	1.634	2.524	1.9080	20.6	3, 4
Q2348−0108	3.01	2.044	2.965	2.4272	20.5	9, 15
	...	...	...	2.6161	21.3	8, 15
Q2351+0217	2.03	1.634	2.000	1.766	20.9	3, 4
Q2359−0216	2.31	1.747	2.779	2.0951	20.7	9, 12
	...	...	...	2.1537	20.3	9, 12

[a] Candidate.

REFERENCES.—(1) Sargent et al. 1989; (2) Savaglio, D'Odorico, & Moller 1994; (3) WLFC95; (4) Virgilio et al. 1995, private communication; (5) Pettini et al. 1994; (6) SMIH96; (7) this paper; (8) Lanzetta et al. 1991; (9) Wolfe et al. 1986; (10) Black, Chaffee, & Foltz 1987; (11) Lu & Wolfe 1994; (12) Wolfe et al. 1993; (13) Lu et al. 1993; (14) Rauch et al. 1990; (15) Turnshek et al. 1989; (16) Storrie-Lombardi & Hook 2000; (17) Lanzetta et al. 1995; (18) SIM96; (19) Francis & Hewett 1993; (20) Sargent, Steidel, & Boksenberg 1988; (21) A. M. Wolfe 1994, private communication.

TABLE 6

STATISTICAL SAMPLE: QSOs WITHOUT DAMPED Lyα ABSORBERS

QSO	z_{em}	z_{min}	z_{max}	Survey Reference
Q0001+0842	3.241	2.024	3.229	1
Q0002+151	1.8990	0.4723	0.6034	2
	...	1.1198	1.5500	2
Q0003+158	0.4500	0.0080	0.4355	2
MG 0004+1359	3.25	1.899	3.207	3
Q0004+1711	2.898	2.002	2.851	1
Q0006+0230	2.09	1.787	2.059	4
Q0006+0200	2.35	1.634	2.317	4
Q0007−0004	2.26	1.634	2.227	4
Q0007−000	2.29	1.670	2.260	5
MG 0007+0141	2.90	1.882	2.861	3
Q0007+106	0.0890	0.0080	0.0781	3
Q0009−0138	1.99	1.634	1.960	4
Q0009+0219	2.66	1.784	2.623	4
Q0009−0215	2.11	1.634	2.079	4
Q0014+8118	3.380	1.928	3.340	1
Q0014−0256	1.85	1.729	1.821	4
Q0015+0239	2.47	1.784	2.435	4
Q0016+0045	2.31	1.651	2.277	4
Q0018−0220	2.56	1.634	2.524	4
Q0018+0047	1.83	1.655	1.802	4
Q0020+0217	1.80	1.665	1.772	4
Q0022+0150	2.77	1.791	2.732	4
Q0023+0010	1.90	1.657	1.871	4
Q0025−0151	2.08	1.634	2.049	4
Q0026+0158	1.89	1.727	1.861	4
Q0026+129	0.1420	0.0080	0.1306	2
Q0027+0149	2.33	1.694	2.297	4
Q0028+0236	2.00	1.634	1.970	4
Q0028−0148	2.08	1.840	2.049	4
Q0029−0152	2.39	2.013	2.356	4
PSS J0030+1702	4.282	2.763	4.229	6
Q0037−018	2.34	1.654	2.303	5
Q0039−2630	1.81	1.634	1.782	4
Q0040−2917	2.09	1.634	2.056	4
Q0041−2638	3.045	1.657	3.029	1
Q0041−2707	2.79	1.668	2.748	4
Q0041−2607	2.79	1.634	2.470	4
Q0041−2658	2.46	1.634	2.422	4
Q0041−2859	2.13	1.589	2.103	4
Q0042−3053	1.97	1.634	1.944	4
Q0042−2627	3.298	2.113	3.253	1
Q0042−2656	3.33	2.215	3.314	1
Q0042−2657	2.90	2.226	2.859	4
Q0043−2937	2.23	1.656	2.198	4
Q0044+030	0.6240	0.3386	0.6078	2
Q0045−3002	2.02	1.603	1.991	4
Q0045−0341	3.138	1.961	3.094	1
Q0045−013	2.53	1.784	2.493	5
Q0046−293	4.014	2.882	3.964	6
BRI B0046−2458	4.15	2.575	4.099	6
Q0047−2759	2.13	1.649	2.099	4
Q0047−3050	2.97	1.930	2.933	4
Q0047−2538	1.97	1.591	1.939	4
Q0047−2326	3.422	2.291	3.378	1
Q0048−0119	1.88	1.634	1.849	4
Q0048−2545	2.08	1.634	2.051	4
Q0049−0104	2.10	1.715	2.065	4
Q0049−0012	1.95	1.634	1.916	4
Q0049+007	2.27	1.644	2.238	5
Q0049+014	2.31	1.681	2.276	5
Q0049+171	0.0640	0.0080	0.0534	2
Q0050+124	0.0611	0.0080	0.0505	2
Q0050−2523	2.16	1.592	2.127	4
Q0051−0226	2.53	1.634	2.491	4
Q1156+295	0.7290	0.0080	0.7117	2
Q1159+0039	2.586	1.671	2.550	1
Q1202+281	0.1650	0.0080	0.1534	2
Q1205−3014	3.036	2.045	2.996	1
Q1206+1155	3.106	2.039	3.073	1
Q1206+1500	2.60	1.793	2.568	4
Q1206+1727	2.36	1.634	2.321	4
Q1206+459	1.1580	0.4231	0.6300	2
	...	0.8426	1.1364	2
Q1209+1046	2.20	1.634	2.163	4
Q1209+1524	3.06	1.634	3.021	4
Q1211+143	0.0850	0.0080	0.0742	2
Q1212+1551	1.95	1.665	1.918	4
Q1212+1045	1.95	1.634	1.922	4
Q1212+0854	2.35	1.634	2.319	4
Q1213+1015	2.52	1.634	2.482	4
Q1213+0922	2.72	1.675	2.681	4
Q1215+1244	2.08	1.634	2.048	4
Q1215+1202	2.83	1.634	2.788	4
Q1215+303	0.2370	0.0080	0.2246	2
Q1216+069	0.3340	0.0080	0.3207	2
Q1216+1517	1.83	1.723	1.802	4
Q1216+1754	1.81	1.634	1.781	4
Q1216+1656	2.83	1.659	2.791	4
Q1216+0947	2.31	1.645	2.279	4
Q1217+023	0.2400	0.0080	0.2276	2
Q1218+304	0.1300	0.0080	0.1187	2
Q1219+755	0.0700	0.0080	0.0593	2
Q1219+1140	2.18	1.634	2.147	4
Q1222+228	2.0400	0.4647	0.6316	2
Q1222+1053	2.30	1.641	2.263	4
Q1223+1059	2.32	1.643	2.288	4
Q1223+1723	2.42	1.659	2.386	4
Q1224+1244	2.14	1.634	2.110	4
Q1225+1512	2.01	1.797	1.977	4
Q1225+1610	2.23	1.663	2.200	4
Q1225+317	2.2190	1.1263	1.5500	2
Q1226+1035	2.32	1.634	2.287	4
Q1226+1115	1.98	1.634	1.950	4
Q1226+1639	2.25	1.634	2.216	4
Q1226+023	0.1580	0.0080	0.1464	2
Q1227+1215	2.17	1.624	2.138	4
Q1228+1808	2.64	1.780	2.607	4
Q1228+077	2.39	1.691	2.354	5
Q1229+1414	2.90	1.764	2.862	4
Q1229+1531	2.27	1.634	2.237	4
Q1229−021	1.0380	0.4738	0.6320	2
Q1229+204	0.0640	0.0080	0.0534	2
Q1230+1042	2.43	1.634	2.396	4
Q1230+1318	2.29	1.634	2.257	4
Q1230+1627B	2.70	1.634	2.663	4
Q1230+0941	1.84	1.641	1.812	4
Q1232−0051	2.78	1.782	2.745	4
Q1232+1139	2.87	1.848	2.831	4
Q1234+0122	2.03	1.634	1.996	4
Q1235+1807A	2.41	1.782	2.371	4
Q1236−0043	1.84	1.690	1.815	4
Q1236−0207	2.25	1.729	2.213	4
Q1237+1515	2.04	1.634	2.009	4
Q1237+0107	1.81	1.733	1.780	4
Q1237+1508	2.07	1.634	2.035	4
Q1237+1212	2.31	1.634	2.281	4
Q1239+1435	1.93	1.634	1.900	4
Q1239+0249	2.22	1.719	2.184	4
Q1240+1504	1.85	1.634	1.823	4

TABLE 6—*Continued*

QSO	z_{em}	z_{min}	z_{max}	Survey Reference
Q0052−0058	2.21	1.634	2.180	4
Q0052+251	0.1550	0.0080	0.1435	2
Q0053−0134	2.06	1.634	2.031	4
Q0053−2824	3.616	2.454	3.576	1
Q0054+0200	1.87	1.634	1.844	4
Q0054+144	0.1710	0.0080	0.1593	2
Q0054−006	2.76	1.854	2.724	5
Q0055+0141	2.23	1.651	2.200	4
Q0055−2744	2.20	1.567	2.163	4
Q0055−2629	3.6560	1.920	3.609	1
Q0055−0200	1.98	1.782	1.953	4
Q0055+0025	1.91	1.634	1.885	4
Q0056−0241	2.23	1.779	2.194	4
Q0057−0225	2.01	1.715	1.979	4
Q0057−274	3.52	2.603	3.475	6
Q0058−2604	2.47	1.606	2.437	4
Q0058−0227	2.23	1.712	2.194	4
Q0058+0155	1.95	1.634	1.924	4
Q0059−0207	2.29	1.653	2.257	4
Q0059−2625	2.10	1.614	2.069	4
Q0059+0035	2.55	1.673	2.510	4
PSS J0059+0003	4.16	2.750	4.108	6
Q0100+0146	1.91	1.692	1.880	4
Q0101−2548	1.97	1.596	1.943	4
Q0101−3025	4.073	1.937	3.116	1
Q0102−0240	1.84	1.731	1.818	4
BRI B0103+0032	4.437	2.87	4.383	7
Q0103−0141	2.21	1.634	2.174	4
Q0103−2901	2.87	1.922	2.831	4
Q0104+0030	1.87	1.667	1.845	4
PC 0104+0215	4.171	2.881	4.119	6
Q0105−2649	2.46	1.667	2.428	4
Q0106−0230	2.28	1.634	2.246	4
Q0106+0119	2.10	1.871	2.068	4
Q0107+0022	1.97	1.634	1.938	4
Q0108+0028	2.01	1.733	1.975	4
Q0109+022	2.35	1.734	2.317	5
Q0110−0107	1.89	1.643	1.860	4
Q0112−2728	2.894	1.784	2.855	1
Q0114−0856	3.163	1.838	3.118	1
Q0115−3002	3.249	1.733	3.207	1
PSS J0117+1552	4.244	2.646	4.192	6
Q0117+213	1.4930	0.9989	1.4681	2
Q0119−286	0.1170	0.0080	0.1058	2
Q0119−013	0.0540	0.0080	0.0435	2
Q0123+257	2.37	1.644	2.338	5
PC 0131+0120	3.792	3.116	3.744	6
Q0132−1947	3.130	1.714	3.089	1
Q0134+329	0.3670	0.0080	0.1050	2
BRI B0135−4239	3.97	2.575	3.920	6
Q0136+010	2.35	1.749	2.317	5
Q0136+1737	2.73	1.632	2.679	1
Q0143−0135	3.141	1.673	3.097	1
GB 0148+2502	3.10	1.825	3.059	3
Q0148−0946	2.850	1.797	2.810	1
BRI B0151−0025	4.194	2.74	4.142	7
Q0153+0430	2.993	1.673	2.951	1
Q0157+001	0.1631	0.0080	0.1515	2
Q0159+036	2.47	1.644	2.436	5
Q0205+024	0.1564	0.0080	0.1448	2
Q0207−0019	2.853	1.756	2.817	1
Q0215+015	1.7150	0.9996	1.5500	2
Q0219+428	0.4440	0.0080	0.4296	2
GB 0229+1309	2.07	1.767	2.039	3
Q0232−042	1.4360	0.0080	0.6320	2
	…	0.8733	1.4116	2
Q1241+176	1.2730	0.4066	0.6320	2
	…	0.7657	1.2503	2
Q1242+0213	1.99	1.634	1.958	4
Q1242+0006	2.08	1.634	2.045	4
Q1242+1732	1.83	1.696	1.805	4
Q1242+1737	1.86	1.634	1.828	4
Q1244+1129	3.16	2.101	3.118	4
Q1244+1642	2.87	1.848	2.826	4
Q1246−0059	2.45	1.669	2.415	4
Q1246+0032	2.31	1.651	2.273	4
Q1247+267	2.0380	0.9211	1.5500	2
Q1248+401	1.0300	0.3984	0.6028	2
	…	0.8919	1.0097	2
Q1253−055	0.5380	0.0080	0.5226	2
Q1259+593	0.4720	0.0080	0.4573	2
Q1302−102	0.2860	0.0080	0.2731	2
Q1307+085	0.1550	0.0080	0.1435	2
Q1308+326	0.9960	0.4670	0.6310	2
Q1308−0214	2.85	1.892	2.811	4
Q1308−0104	2.59	1.634	2.549	4
Q1309+355	0.1840	0.0080	0.1722	2
Q1312+043	2.35	1.813	2.319	5
Q1313+0107	2.39	1.647	2.359	4
PSS J1317+3531	4.365	2.978	4.311	6
Q1317+277	1.0220	0.2503	1.0018	2
Q1318+290B	0.5490	0.3757	0.5335	2
Q1318−0150	2.01	1.651	1.980	4
Q1318−113	2.3080	1.896	2.273	5
Q1320+0048	1.96	1.655	1.925	4
Q1323−0248	2.12	1.661	2.090	4
Q1324−0212	1.89	1.634	1.857	4
Q1327−206	1.1690	1.1243	1.1473	2
Q1328+0223	2.15	1.937	2.122	4
BRI B1328−0433	4.217	2.24	4.165	7
Q1329+0231	2.43	1.663	2.400	4
Q1329+0018	2.35	1.661	2.318	4
Q1331+170	2.0840	1.2621	1.5500	2
Q1333+176	0.5540	0.3902	0.5385	2
Q1334+246	0.1070	0.0080	0.0959	2
Q1334−0033	2.78	1.634	2.745	4
Q1334+0212	2.38	1.634	2.350	4
BRI B1335−0417	4.396	3.08	4.342	7
Q1336+0210	1.96	1.634	1.932	4
GB 1338+3809	3.10	1.737	3.059	3
Q1338+101	2.45	1.724	2.412	5
Q1338+416	1.2190	0.4066	0.6324	2
	…	0.8684	1.1968	2
Q1340+0959	2.942	1.894	2.897	1
Q1344+0137	1.92	1.634	1.886	4
Q1345−0137	1.93	1.634	1.900	4
Q1345−0120	2.95	1.926	2.906	4
Q1346+0121A	1.93	1.634	1.901	4
Q1346−036	2.36	1.653	2.327	5
Q1351+640	0.0880	0.0080	0.0771	2
Q1352+183	0.1520	0.0080	0.1405	2
Q1352+108	3.18	1.928	3.137	5
Q1353+186	0.0505	0.0080	0.0400	2
Q1354+195	0.7200	0.3593	0.6330	2
Q1355−416	0.3130	0.0080	0.2999	2
Q1356+581	1.3710	0.5218	0.6310	2
Q1358+115	2.59	1.677	2.550	5
Q1358+3908	3.3	2.221	3.237	1
Q1400+0935	2.980	2.022	2.930	1
Q1402−012	2.52	1.789	2.479	5
Q1402+044	3.20	2.340	3.160	5
Q1406+123	2.94	2.018	2.903	5

TABLE 6—*Continued*

QSO	z_{em}	z_{min}	z_{max}	Survey Reference
Q0237−233	2.2230	1.1593	1.5402	2
Q0239−1527	2.786	1.928	2.744	1
BRI B0241−0146	4.053	2.86	4.002	7
BR B0245−0608	4.238	2.96	4.186	7
PSS J0248+1802	4.43	2.810	4.376	6
Q0249−1826	3.210	1.871	3.163	1
Q0249−2212	3.21	2.044	3.160	8, 6
Q0252+0136	2.47	1.634	2.430	4
Q0254+0000	2.25	1.634	2.215	4
Q0256−0000	3.377	2.241	3.330	1
Q0256−0031	2.00	1.634	1.965	4
Q0258+0210	2.52	1.634	2.489	4
Q0301−0035	3.226	2.060	3.181	1
Q0302−0019	3.290	1.739	3.243	1
Q0302−223	1.4000	1.0077	1.3760	2
Q0305+0127	2.15	1.634	2.118	4
Q0307−0058	2.11	1.634	2.075	4
Q0308+0129	2.34	1.739	2.302	4
Q0308+1902	2.839	1.673	2.797	1
Q0308−1920	2.756	1.673	2.714	1
Q0312−770	0.2230	0.0080	0.2108	2
Q0316−2023	2.869	1.747	2.826	2
Q0323+022	0.1470	0.0080	0.1295	2
Q0329−2534	2.689	1.661	2.662	1
Q0334−2029	3.132	2.057	3.089	1
PC 0345+0130	3.638	2.699	3.592	6
BR B0351−1034	4.351	3.09	4.297	7
Q0351−3904	3.01	1.632	2.970	1
Q0352−2732	2.823	1.673	2.781	1
BR B0401−1711	4.236	2.82	4.184	7
Q0405−123	0.5740	0.0080	0.5583	2
Q0414−060	0.7810	0.0080	0.7632	2
Q0420+007	2.918	1.673	2.879	1
Q0420−3851	3.1230	2.094	3.082	1
Q0428−1342	3.244	1.965	3.200	1
Q0454−220	0.5340	0.1199	0.5187	2
Q0454+039	1.3450	0.9672	1.3216	2
Q0457+024	2.38	1.645	2.346	5
MG 0504+0303	2.46	1.803	2.425	3
Q0521−365	0.0566	0.0080	0.0460	2
Q0537−441	0.8940	0.5139	0.6300	2
Q0548−322	0.0690	0.0080	0.0583	2
Q0552+398	2.36	1.644	2.325	5
Q0558−504	0.1370	0.0080	0.1256	2
Q0624+691	0.3700	0.0080	0.3563	2
Q0636+6801	3.178	2.019	3.132	1
Q0637−752	0.6560	0.0080	0.6251	2
Q0642+4454	3.408	2.192	3.362	1
Q0702+646	0.0795	0.0080	0.0687	2
Q0731+6519	3.038	2.019	2.993	1
Q0735+178	0.4240	0.0765	0.4098	2
Q0736+017	0.1910	0.0080	0.1791	2
Q0742+318	0.4620	0.0080	0.4474	2
Q0743−673	1.5130	1.0302	1.4879	2
GB 0749+4239	3.59	2.185	3.544	3
PC 0751+5623	4.281	3.526	4.228	6
Q0754+100	0.6700	0.0080	0.6257	2
Q0754+394	0.0958	0.0080	0.0848	2
Q0804+761	0.1000	0.0080	0.0890	2
Q0805+0441	2.880	1.838	2.834	1
Q0812+332	2.42	1.677	2.385	5
Q0819−032	2.35	1.704	2.319	5
Q0820+296	2.37	1.644	2.333	5
MG 0830+1009	3.75	2.040	3.703	3
Q0830+1133	2.979	1.797	2.936	1
Q0831+1238	2.748	1.961	2.706	1
Q1407+265	0.9440	0.0080	0.9246	2
Q1410+096	3.21	2.099	3.169	5
Q1411+442	0.0900	0.0080	0.0791	2
GB 1413+3720	2.36	1.735	2.326	3
Q1415+451	0.1140	0.0080	0.1029	2
Q1416−129	0.1290	0.0080	0.1177	2
Q1418+546	0.1520	0.0080	0.1405	2
Q1419+480	0.0720	0.0080	0.0613	2
Q1421+330	1.9040	1.0311	1.5500	2
Q1425+267	0.3620	0.2409	0.3484	2
Q1426+015	0.0860	0.0080	0.0751	2
Q1428+0202	2.11	1.634	2.075	4
Q1429−0053	2.08	1.719	2.047	4
Q1429+118	3.00	1.958	2.963	5
PSS J1430+2828	4.306	2.777	4.253	6
Q1433+0223	2.14	1.634	2.111	4
Q1433−0025	2.04	1.634	2.012	4
PSS J1435+3057	4.297	2.905	4.244	6
GB 1436+4431	2.10	1.769	2.069	3
Q1439+0047	1.86	1.649	1.828	4
Q1440−0024	1.81	1.634	1.786	4
Q1440+356	0.0781	0.0080	0.0673	2
Q1444+407	0.2670	0.0080	0.2543	2
Q1444+0126	2.21	1.717	2.174	4
Q1444−0112	2.15	1.651	2.121	4
Q1451−375	0.3140	0.0080	0.3009	2
Q1455+123	3.08	1.830	3.033	5
MG 1500+0431	3.67	2.606	3.623	6
Q1503+118	2.78	1.957	2.740	5
GB 1508+5714	4.283	2.73	4.230	7
Q1512+370	0.3710	0.0080	0.3573	2
MG 1519+1806	3.06	1.955	3.019	3
GB 1520+4347	2.18	1.775	2.148	3
Q1522+101	1.3210	0.0080	0.6310	2
	...	0.8803	1.2978	2
Q1525+227	0.2530	0.0080	0.2405	2
GB 1526+6701	3.02	1.955	2.980	3
Q1526+285	0.4500	0.0080	0.2428	2
Q1538+477	0.7700	0.3326	0.6326	2
Q1545+210	0.2640	0.0080	0.2514	2
Q1548+0917	2.749	1.874	2.707	1
PC 1548+4637	3.544	2.607	3.499	6
Q1553+113	0.3600	0.0080	0.3464	2
Q1556+273	0.0899	0.0080	0.0790	2
MG 1557+0313	3.891	2.66	3.842	7
MG 1559+1405	2.24	1.737	3.059	3
Q1600+0729	4.38	3.062	4.326	6
Q1607+1819	3.123	1.814	3.0918	1
Q1612+261	0.1310	0.0080	0.1197	2
Q1613+658	0.1290	0.0080	0.1177	2
Q1623+268A	2.47	1.644	2.433	5
Q1623+268B	2.54	1.644	2.502	5
Q1630+377	1.4710	0.0080	0.6320	2
	...	0.8641	1.4463	2
Q1631+3722	2.940	1.785	2.906	1
Q1634+706	1.3340	0.5547	1.3107	2
Q1641+399	0.5950	0.0080	0.5791	2
PC 1640+4628	3.700	2.604	3.653	6
Q1704+608	0.3710	0.0080	0.3573	2
Q1705+0152	2.576	1.669	2.537	1
Q1715+535	1.9290	1.1009	1.5500	2
Q1718+481	1.0840	0.0080	1.0632	2
Q1721+343	0.2060	0.0080	0.1939	2
Q1726+3425	2.429	1.669	2.393	1
Q1727+502	0.0550	0.0080	0.0445	2
Q1738+3502	3.240	2.093	3.197	1

TABLE 6—*Continued*

QSO	z_{em}	z_{min}	z_{max}	Survey Reference
Q0837−120	0.1980	0.0080	0.1860	2
Q0844+349	0.0640	0.0080	0.0534	2
Q0846+152	2.64	1.831	2.599	5
MG 0848+1533	2.01	1.735	1.980	3
Q0849+080	0.0620	0.0080	0.0514	2
Q0851+202	0.3060	0.0080	0.2929	2
Q0855+182	2.62	1.682	2.580	5
Q0903+155	2.68	1.659	2.645	5
MG 0906+0406	3.20	1.811	3.158	3
Q0906+484	0.1180	0.0080	0.1068	2
Q0910+403	0.9360	0.0080	0.9166	2
Q0914−621	0.0573	0.0080	0.0467	2
Q0916+555	0.1235	0.0080	0.1123	2
Q0932+3646	2.84	1.634	2.814	1
Q0933+733	2.53	1.651	2.493	5
Q0938+1159	3.19	1.634	3.149	1
Q0941+2608	2.913	1.731	2.867	1
Q0953+414	0.2390	0.0080	0.2266	2
Q0955+326	0.5330	0.0080	0.5177	2
Q0956+1217	3.306	2.159	3.263	1
Q0957+561	1.4050	0.8179	1.3810	2
Q0958+551	1.7324	1.1762	1.4513	2
Q1001+291	0.3290	0.0080	0.3157	2
Q1004+130	0.2410	0.0080	0.2286	2
Q1004+1411	2.707	1.786	2.672	1
Q1007+417	0.6110	0.0080	0.5949	2
Q1009−0252	2.75	1.651	2.708	4
Q1011−282	0.6110	0.0080	0.1310	2
Q1011−0144	2.24	1.669	2.204	4
Q1011+250	1.6310	0.9718	1.5500	2
Q1012+008	0.1850	0.0080	0.1732	2
Q1012−0206	2.14	1.634	2.104	4
GB 1013+2052	3.11	1.945	3.069	3
Q1014+0023	2.29	1.634	2.591	4
Q1016−0039	2.18	1.649	2.144	4
Q1017+1055	3.158	2.114	3.127	1
Q1017+280	1.9280	0.9971	1.4678	2
Q1018−0005	2.60	1.789	2.560	4
Q1020+0028	1.90	1.680	1.872	4
Q1021−0037	2.547	1.887	2.513	1
Q1024+0030	2.17	1.717	2.135	4
Q1025−0030	2.87	1.885	2.833	4
Q1028+313	0.1770	0.0080	0.1652	2
Q1029−140	0.0860	0.0080	0.0751	2
Q1033+1342	3.07	1.800	3.048	1
BR B1033−0327	4.509	2.91	4.454	7, 9
Q1038+528	2.30	1.677	2.262	5
GB 1041+3014	2.99	1.735	2.950	3
Q1047+550	2.1650	1.3299	1.5159	2
BRI B1050−0000	4.286	2.83	4.233	7
Q1100+772	0.3110	0.0080	0.2979	2
Q1100−264	2.1450	1.1551	1.5500	2
MG 1101+0248	2.51	1.736	2.475	3
Q1103−006	0.4260	0.0080	0.4117	2
BRI B1110+0106	3.918	2.58	3.869	7
Q1115+080	1.7180	0.4066	0.6330	2
	...	0.9595	1.5500	2
Q1116+215	0.1770	0.0080	0.1652	2
Q1123+264	2.35	1.645	2.317	5
Q1124+5706	2.890	1.762	2.851	1
Q1127+078	2.66	1.644	2.621	5
Q1128+105	2.65	2.040	2.610	5
Q1131−0043	2.16	1.653	2.128	4
Q1132−0054	2.76	1.717	2.718	4
Q1135−0255	2.41	1.739	2.373	4
Q1136−135	0.5570	0.0080	0.5414	2
GB 1745+6227	3.901	2.47	3.852	7
Q1803+676	0.1360	0.0080	0.1246	2
Q1807+698	0.0512	0.0080	0.0407	2
Q1821+643	0.2970	0.0080	0.2840	2
Q1831+731	0.1230	0.0080	0.1118	2
Q1833+326	0.0590	0.0080	0.0484	2
Q1836+5108	2.827	1.920	2.789	1
Q1839−785	0.0743	0.0080	0.0636	2
Q1845+797	0.0556	0.0080	0.0450	2
Q1912−550	0.4020	0.1769	0.2041	2
Q1928+738	0.3020	0.0080	0.2890	2
PKS 1937−101	3.787	2.442	3.739	1
Q2000−3300	3.783	2.521	3.729	1
Q2005−489	0.0710	0.0080	0.0603	2
Q2038−0116	2.783	1.887	2.745	1
Q2045−377	1.8000	1.0040	1.5500	2
Q2048+3116	3.198	1.830	3.143	1
Q2050−359	3.49	2.605	3.445	6
Q2113−4345	2.05	1.664	2.023	4
Q2113−4534	2.54	1.969	2.506	4
Q2114−4346	2.04	1.606	2.011	4
Q2115−4434	2.16	1.755	2.128	4
Q2117−4703	2.26	1.849	2.223	4
Q2122−4231	2.27	1.550	2.233	4
Q2126−1551	3.2660	2.011	3.218	1
Q2126−4618	1.89	1.715	1.859	4
Q2127−4528	2.71	2.018	2.676	4
Q2128−123	0.5010	0.0940	0.4860	2
Q2130+099	0.0610	0.0080	0.0504	2
Q2131−4257	2.10	1.590	2.065	4
Q2134−4239	1.80	1.590	1.776	4
Q2134−147	0.2000	0.0080	0.1880	2
Q2135−4632	2.21	1.879	2.182	4
Q2136+141	2.43	1.784	2.390	5
Q2139−4434	3.23	2.373	3.188	4
Q2141+175	0.2130	0.0080	0.2009	2
Q2145+067	0.9900	0.9426	0.9701	2
MG 2152+1420	2.56	1.800	2.524	3
Q2153−2056	1.85	1.634	1.821	4
Q2155−304	0.1170	0.0080	0.1058	2
Q2159−2058	2.12	1.634	2.089	4
Q2201+315	0.2970	0.0080	0.2840	2
Q2203−2145	2.27	1.692	2.240	4
Q2203−1833	2.73	1.849	2.691	4
Q2205−2014	2.64	1.652	2.599	4
MG 2206+1753	3.14	1.769	3.099	3
Q2209−1842	2.09	1.634	2.061	4
Q2209+184	0.0700	0.0080	0.0593	2
Q2211−1915	1.95	1.634	1.923	4
BR B2212−1626	3.990	2.69	3.940	7
Q2214+139	0.0658	0.0080	0.0551	2
MG 2222+0511	2.32	1.800	2.287	3
GB 2223+2024	3.56	2.101	3.514	3
Q2231+0125	1.90	1.634	1.871	4
Q2231−0212	1.90	1.634	1.871	4
Q2233+1341	3.209	2.216	3.167	1
Q2233+1310	3.298	2.134	3.252	1
Q2241+0014	2.14	1.657	2.099	4
Q2243+0141	2.30	1.663	2.267	4
Q2244−0234	1.97	1.787	1.940	4
Q2244−0105	2.04	1.634	2.010	4
Q2246−0006	2.05	1.651	2.019	4
BR B2248−1242	4.161	2.94	4.109	7
MG 2251+2429	2.33	2.019	2.297	3
Q2251−178	0.0680	0.0080	0.0573	2
Q2251+113	0.3230	0.1310	0.3098	2

TABLE 6—*Continued*

QSO	z_{em}	z_{min}	z_{max}	Survey Reference	QSO	z_{em}	z_{min}	z_{max}	Survey Reference
Q1136+122.....	2.90	1.781	2.862	5	MG 2254+0227.....	2.09	2.767	2.059	3
Q1137+660.....	0.6460	0.0080	0.6295	2	Q2256+017	2.67	1.786	2.629	5
Q1138−0107	2.76	1.953	2.718	4	Q2302+029	1.0440	0.3942	0.6290	2
Q1139−0139	1.93	1.634	1.884	4		...	0.8060	1.0236	2
Q1139−0037	1.91	1.634	1.896	4	Q2308+098	0.4320	0.0080	0.4177	2
Q1142+0138	2.42	1.791	2.390	4	Q2311−0341	3.048	1.714	3.001	1
Q1142+1015	3.152	2.127	3.109	1	MG 2320+0755.....	2.09	1.780	2.059	3
Q1143+0142	2.28	1.634	2.248	4	Q2326−477	1.2990	0.9164	1.2760	2
Q1143+099.....	2.60	1.676	2.567	5	PC 2331+0216.....	4.093	3.115	4.042	6
Q1144+115.....	2.51	1.682	2.471	5	Q2334+1041	2.243	1.634	2.211	1
Q1144+0140	2.59	1.667	2.551	4	Q2344+092	0.6720	0.0080	0.6288	2
Q1145−0039	1.94	1.634	1.912	4	Q2351+1042	2.379	1.632	2.345	1
Q1145+0121	2.08	1.721	2.045	4	Q2351+0120	2.07	1.634	2.039	4
Q1146+0207	2.06	1.634	2.025	4	Q2351−1154	2.67	1.632	2.633	1
Q1147+084.....	2.61	1.854	2.577	5	Q2352+0205	2.19	1.634	2.158	4
GB 1147+4348.....	3.02	2.035	2.980	3	Q2354−0134	2.21	1.665	2.178	4
Q1148−0007	1.977	1.634	1.947	4	Q2356+0139	2.07	1.661	2.039	4
Q1148+0055	1.89	1.667	1.858	4	Q2356+0237	2.50	1.634	2.465	4
Q1148+549.....	0.9690	0.0080	0.9493	2	Q2359+0653	3.238	1.632	3.203	1
Q1151+117.....	0.1760	0.0080	0.1642	2	Q2359+0023	2.897	1.714	2.857	1

REFERENCES.—(1) Lanzetta et al. 1991; (2) Lanzetta et al. 1995; (3) Storrie-Lombardi & Hook 2000; (4) WLFC95; (5) Wolfe et al. 1986; (6) this paper; (7) SMIH96; (8) Sargent et al. 1989; (9) SIM96.

where Θ is the Heaviside step function, and where the sum is over the m QSOs in the survey (see Lanzetta et al. 1991).

The left panel of Figure 5 illustrates how the redshift sensitivity for the entire statistical sample compares with previous work. The data included in this paper are shown as a solid line; the large compilation of damped systems in the Large Bright Quasar Survey (WLFC95), which provides the bulk of the data for $z < 3$, is shown as a dashed line; and the Automated Place Measuring Facility (APM) survey (SMIH96), which provided most of the previous data for $z > 3$, is shown as a dotted line. The right panel of Figure 5 shows the detail for the redshift range $z \geq 3$.

The new data included in this paper increase by 75% the redshift path surveyed for $z \geq 3$. In Table 7 we compare Δz

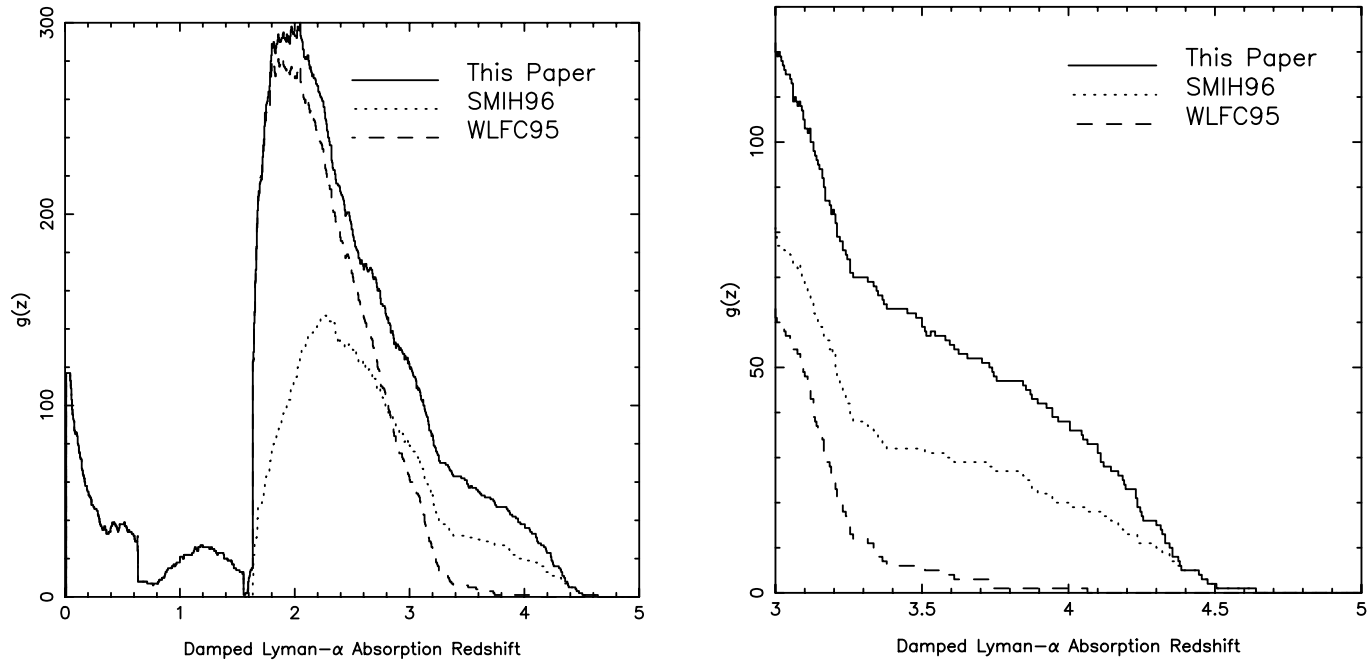

FIG. 5.—Redshift sensitivity function, $g(z)$, plotted for the combined data sets used in this survey as a solid line. Shown are the number of lines of sight at a given redshift over which damped systems can be detected at a $>5\,\sigma$ level. Left panel illustrates how the redshift sensitivity for the entire statistical sample compares with previous work. The data included in this paper are shown as a solid line, the large compilation in the LBQS survey (WLFC95), which provides the bulk of the data for $z < 3$, is shown as a dashed line, and the APM survey (SMIH96), which provided most of the previous data for $z > 3$, is shown as a dotted line. Right panel shows the detail for the redshift range $z \geq 3$. The new data included in this paper nearly double the redshift path previously surveyed for $z \geq 3$.

TABLE 7

REDSHIFT PATH SURVEYED

REDSHIFT RANGE	SURVEY	Δz	ΔX ($q_0 = 0$)	ΔX ($q_0 = 0.5$)	NUMBER OF QSOs
3.00–5.00	This paper	73.8	332.5	156.5	128
	APM	43.5	195.8	92.2	82
	LBQS	13.4	56.3	27.5	61
0.01–5.00	This paper	418.4	1364.2	747.6	645
	APM	239.5	764.4	421.3	366
	LBQS	323.8	966.8	554.1	571

REFERENCES.—APM: SMIH96; LBQS: WLFC95.

for the Large Bright Quasar Survey (LBQS), the APM survey, and this paper for $z > 3$ and for the entire redshift range of the samples. We also give analogous values for the total "absorption distance," ΔX, which is defined as

$$X(z) = \begin{cases} \frac{2}{3}[(1+z)^{3/2} - 1] & \text{if } q = 0.5\ , \\ \frac{1}{2}[(1+z)^2 - 1] & \text{if } q = 0.0\ . \end{cases} \quad (2)$$

(Bahcall & Peebles 1969; cf. Tytler 1987). The redshift path over which damped systems could be detected is crucial in estimating the cosmological mass density in neutral gas from the damped systems, as well as the number density per unit redshift and the frequency distribution per unit column density. These are discussed in detail in the next section.

4. ANALYSIS

4.1. *Frequency Distribution of Column Densities, $f(N, z)$*

By combining our statistical sample of damped systems with the data presented in Hu et al. (1995) for column densities $N_{\rm H\,I} \leq 2 \times 10^{20}$ atoms cm^{-2}, we can examine the frequency distribution for the entire H I column density range, 10^{12}–10^{22} atoms cm^{-2} (see Tytler 1987; Petitjean et al. 1993; Hu et al. 1995). This is shown in Figure 6. To first order, it is fitted by a power-law function, $f(N) \propto N^{-1.46}$, over 10 orders of magnitude in column density. The Lyα forest absorbers are by far the most numerous, yet if we integrate this to find the mass density, the bulk of the H I mass is locked up in the damped systems. A disadvantage of a power-law model for the H I column density distribution of damped Lyα absorbers is the divergent nature of the integral mass contained in the systems. A high column density cutoff (e.g., 10^{22}) must be selected to perform the integral. We discuss below an alternative parameterization based on a gamma distribution (cf. Pei & Fall 1995; SIM96).

4.1.1. *Differential Column Density Distribution*

The frequency distribution of H I column densities is defined as follows. Let $f(N, X)dN\,dX$ be the number of absorbers per sight line, with H I column densities in the interval $(N, N + dN)$, and absorption distances in the interval $(X, X + dX)$. Then the frequency distribution of H I column densities is $f(N, z) \equiv f(N, X[z])$. In Figure 7 we show the $f(N, z)$ derived from the entire statistical sample of damped absorbers for $q_0 = 0.0$, and in Figure 8 we show the same data divided into four redshift bins: $z = 0.008$–1.5, 1.5–2.5, 2.5–3.5, and 3.5–4.7. The flattest distribution is in the redshift range $z = 3.0$–3.5, and it steepens toward higher and lower redshifts from this point. This was noted in WLFC95 for the $z < 3.5$ data and in SIM96 for the $z > 3.5$ data, but the differences in $f(N)$ with redshift were not statistically significant. Our new statistical sample is large enough to make some quantitative statements about the redshift evolution of $f(N)$ at high redshift.

4.1.2. *The Neutral Gas Density at $z < 1.5$*

There is a steepening of the differential distribution of column densities evident at $z < 1.5$ in our data set, but not at a statistically significant level. Previous surveys have shown a very low number density per unit redshift from *International Ultraviolet Explorer* (*IUE*) and *Hubble Space Telescope* (*HST*) data (LWT95), and Jannuzi et al. (1998) also find numbers consistent with this from *HST* Key Project data. However, Rao & Turnshek (1998) have reported in a Letter the discovery of 12 new low-redshift damped systems, and their full survey has just appeared in preprint form (Rao & Turnshek 2000). This redshift range is problematic, because any bias in QSO surveys due to possible obscuration by dust in foreground absorbers would have the largest impact here (see Pei & Fall 1995; SMI96). In this paper we focus on the redshift range $z > 1.5$.

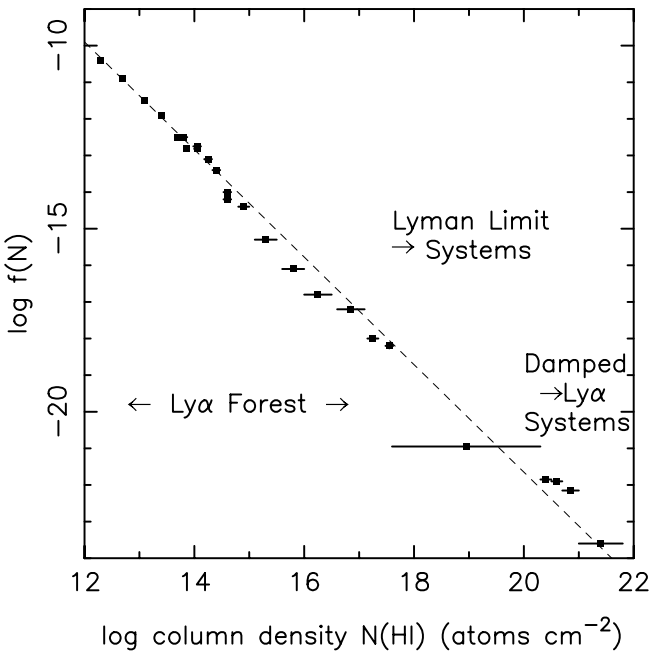

FIG. 6.—Column density distribution function of neutral hydrogen for the $12 \leq \log N_{\rm H\,I} \leq 22$ damped Lyα absorbers. To first order, it is fitted by a power law, $f(N) \propto N^{-1.46}$, over 10 orders of magnitude in column density.

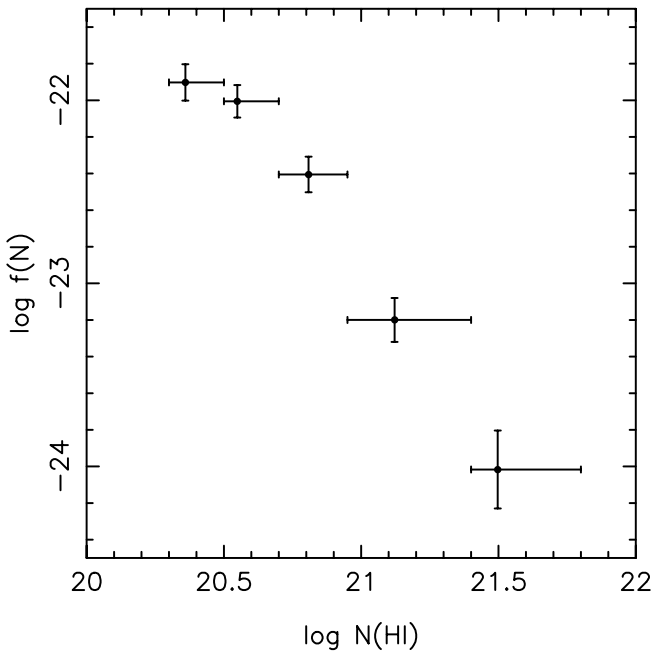

FIG. 7.—Differential column density distribution function of neutral hydrogen determined for the entire statistical sample of damped Lyα absorbers.

4.1.3. *Evolution of the Neutral Gas Density at $z > 1.5$*

For the first time, we determine a *statistically significant* (greater than 99.7% confidence) steepening in the column density distribution function at redshifts $z > 4.0$. This is evidenced by comparing the data in the redshift range $1.5 < z < 4$ with the data at $z \geq 4$, as shown in Figure 9. This shows the cumulative distribution, normalized by the absorption distance surveyed. A Kolmogorov-Smirnov (K-S) test gives a probability of only 0.006 that the two redshift samples are drawn from the same distribution. The steepening of the distribution function is due to both fewer very high column density absorbers ($N_{\rm H\,I} \geq 10^{21}$ atoms cm^{-2}) and more lower column density systems ($N_{\rm H\,I} = 2$–4×10^{20}). No damped systems with column densities log $N_{\rm H\,I} \geq 21$ have yet been detected at $z > 4$.

4.1.4. *Fits to the Column Density Distribution*

A single power law, $f(N) = kN^{-\beta}$, does not provide a good fit to the column density distribution function for damped Lyα absorbers. A single power-law fit has the additional problem that if $\beta < 2$, as all current estimates indicate, then the total mass in damped systems diverges unless an upper bound to the H I column density is assumed. An alternative parameterization, using a gamma function to describe the H I column density distribution, was suggested

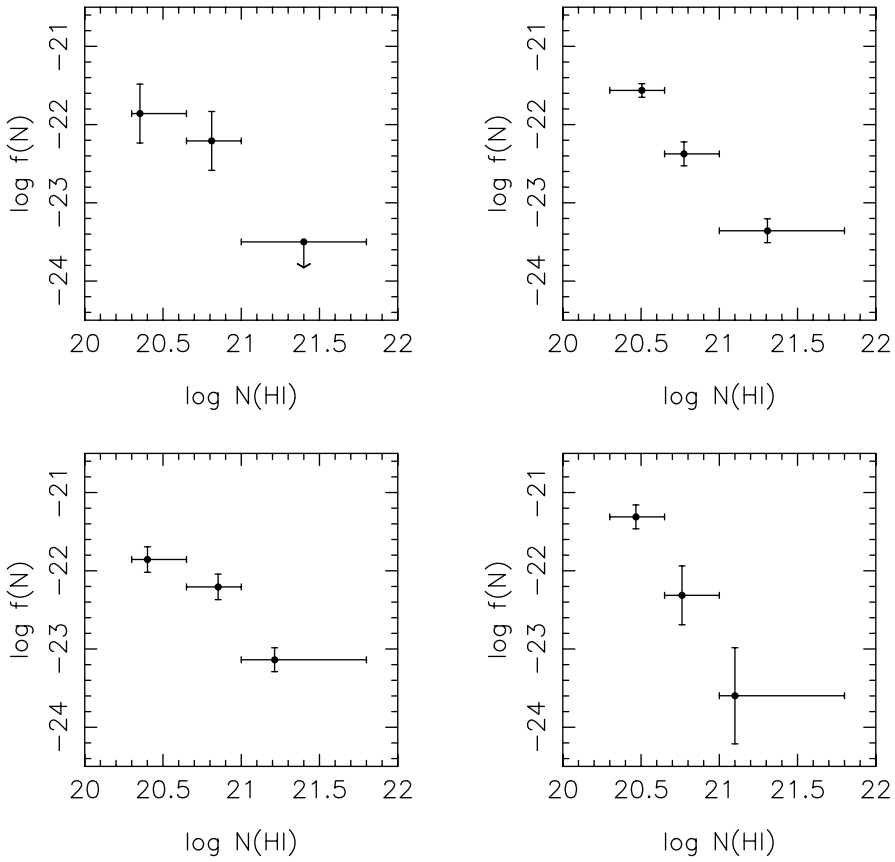

FIG. 8.—Differential column density distribution function of neutral hydrogen for damped Lyα absorbers shown in four redshifts bins: 0.008–1.5 (*top left*), 1.5–2.5 (*top right*), 2.5–3.5 (*bottom left*), and 3.5–4.7 (*bottom right*). The distribution is flattest at $z \approx 3$ and steepens toward higher and lower redshifts from that point. The steepening at high redshift is due to both a paucity of very high column density systems and an increase in the frequency of lower column density systems. There is also a steepening of the differential distribution evident at $z < 1.5$, but this is not statistically significant (see Rao & Turnshek 2000 for new results in this redshift range).

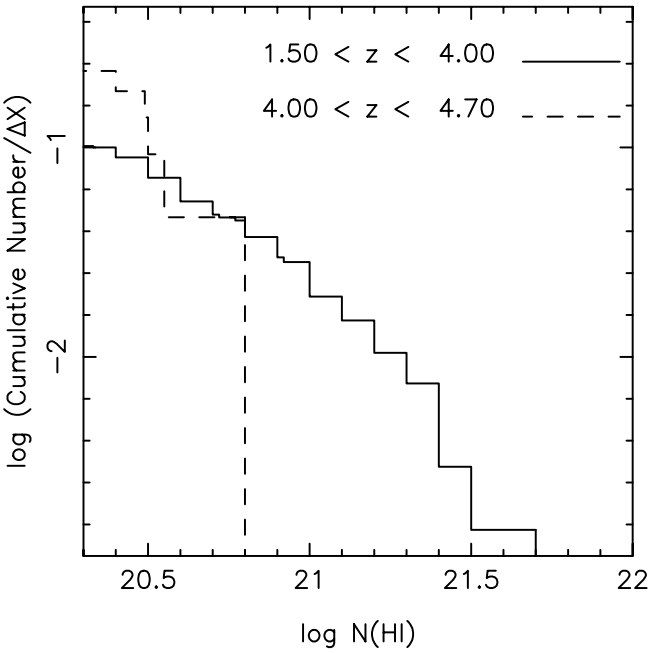

FIG. 9.—The log of the cumulative number of damped Lyα absorbers vs. log column density normalized by the redshift path surveyed, shown versus log column density for two redshift ranges. Solid lines shows the data for $1.5 < z < 4.0$, and dashed line shows the data for $z \geq 4.0$. A K-S test gives a probability of only 0.006 that the two redshift samples are drawn from the same distribution. This is the first time that the steepening of the column density distribution function has been shown to be statistically significant.

by Pei & Fall (1995) and adopted by SIM96. We use the same formalism here.

We model the data with a gamma distribution of the form

$$f(N, z) = \frac{f_*}{N_*}\left(\frac{N}{N_*}\right)^{-\beta} e^{-N/N_*}\,, \tag{3}$$

where f_* is the characteristic number of absorbing systems at the column density N_*, and N_* is a parameter defining the turnover, or "knee," in the number distribution. Both f_* and N_* may in general vary with redshift, but for the moment we treat them as constants. This functional form is similar to the Schechter luminosity function (Schechter 1976). For $N \ll N_*$, the gamma function tends to the same form as the single power law, $f(N) \propto N^{-\beta}$, while for $N \gtrsim N_*$ the exponential term begins to dominate. We use a maximum-likelihood technique to find a solution over a two-dimensional grid of pairs of values of N_* and β, since the constant f_* can be directly computed using the constraint

$$m = \sum_{i=1}^{n} f_* \int_{N_{\min}}^{N_{\max}} \int_{z^i_{\min}}^{z^i_{\max}} f(N, z)dz\,dN\,, \tag{4}$$

where m is the total number of observed systems.

The results of fits to the data in the redshift ranges $1.5 < z < 4$ and $z \geq 4$, overplotted on the cumulative distribution of absorbers, are shown in the top panels of Figure 10. A data point for the expected number of Lyman-limit systems that would be detected down to log $N_{\rm H\,I} = 17.2$ is shown by a circled star. Lyman-limit systems are defined and detected by the observation of neutral hydrogen (H I) absorption, which is optically thick to Lyman-continuum radiation for $\lambda < 912$ Å, the Lyman limit, corresponding to a column density $N(\text{H I}) \geq 1.6 \times 10^{17}$ cm^{-2} (see Tytler 1982; Sargent, Steidel, & Boksenberg 1989; Lanzetta 1991; Storrie-Lombardi et al. 1994; Stengler-Larrea et al. 1995 for discussions of Lyman-limit systems). Their contribution is calculated by integrating the number density per unit redshift of Lyman-limit systems expected $[N(z) = 0.27(1 + z)^{1.55}]$ over the redshift path covered by the n QSOs in the damped sample, i.e.,

$$\begin{aligned}\text{LLS}_{\text{expected}} &= \sum_{i=1}^{n} \int N(z)dz = \sum_{i=1}^{n} \int_{z_{\min}}^{z_{\text{em}}} N_0(1 + z)^{\gamma}\,dz \\ &= \sum_{i=1}^{n} \int_{z_{\min}}^{z_{\text{em}}} 0.27(1 + z)^{1.55}\,dz \end{aligned} \tag{5}$$

(SMIH94; SIM96). Including the Lyman-limit system point provides a longer baseline in column density and allows us to make better estimates of the uncertainties in the fit. The log-likelihood function results, with confidence contours, are shown in the bottom panels of Figure 10.

The parameters for the fit in equation (3) are very similar for both redshift ranges when the Lyman-limit systems are included, with log $N_* = 21.22$ atoms cm^{-2} for both, $\beta = 1.24, f_* = 0.05$ for the lower redshift data, and $\beta = 1.08$, $f_* = 0.16$ for the higher redshift data. Without the Lyman-limit point anchoring the lower column density end, the fits to just the high column density damped systems yield $\beta = 1.52 \pm 0.25$, $f_* = 0.03$, and log $N_* = 21.39 \pm 0.30$ for the lower redshift data and $\beta = 0.32 \pm 0.6$, $f_* = 0.34$, and log $N_* = 20.92 \pm 0.50$ for the higher redshift data. The errors on the exponent β are very large for the $z > 4$ data, due to the small number of data points. The fits reflect what we saw in looking at the differential counts, i.e., the "knee," N_*, where the distribution turns over is at a lower column density for the higher redshift data. The best-fit results are tabulated in Table 8.

In SIM96, with a much smaller data set (366 QSOs, 44 absorbers), we obtained log $N_* = 21.63 \pm 0.35$, $\beta = 1.48 \pm 0.30$, and $f_* = 1.77 \times 10^{-2}$, fitting the whole sample. With our current statistical sample (646 QSOs, 85 absorbers), we find very similar results, with $N_* = 21.33 \pm 0.30$, $\beta = 1.48 \pm 0.25$, and $f_* = 3.19 \times 10^{-2}$. Alternatively, single power-law fits of the form $f(N) \propto N^{-\beta}$ (not including the point for the Lyman-limit systems) yield $\beta = 1.96$ for $z > 4$ and $\beta = 1.78$ for $1.5 < z < 4$, again consistent with values obtained in earlier work (Lanzetta et al. 1991; SIM96).

TABLE 8

FIT TO H I COLUMN DENSITY DISTRIBUTION, $f(N, z) = (f_*/N_*)(N/N_*)^{-\beta}e^{-N/N_*}$

Redshift Range	f_*	log N_*	β
Including Lyman-Limit System Data			
1.5–4.0.....	0.051	$21.22^{+0.10}_{-0.16}$	$1.24^{+0.02}_{-0.08}$
4.0–4.7.....	0.160	$21.22^{+0.52}_{-0.33}$	$1.08^{+0.14}_{-0.22}$
Not Including Lyman-Limit System Data			
1.5–4.0.....	0.03	21.39 ± 0.30	1.52 ± 0.25
4.0–4.7.....	0.34	20.92 ± 0.50	0.32 ± 0.60

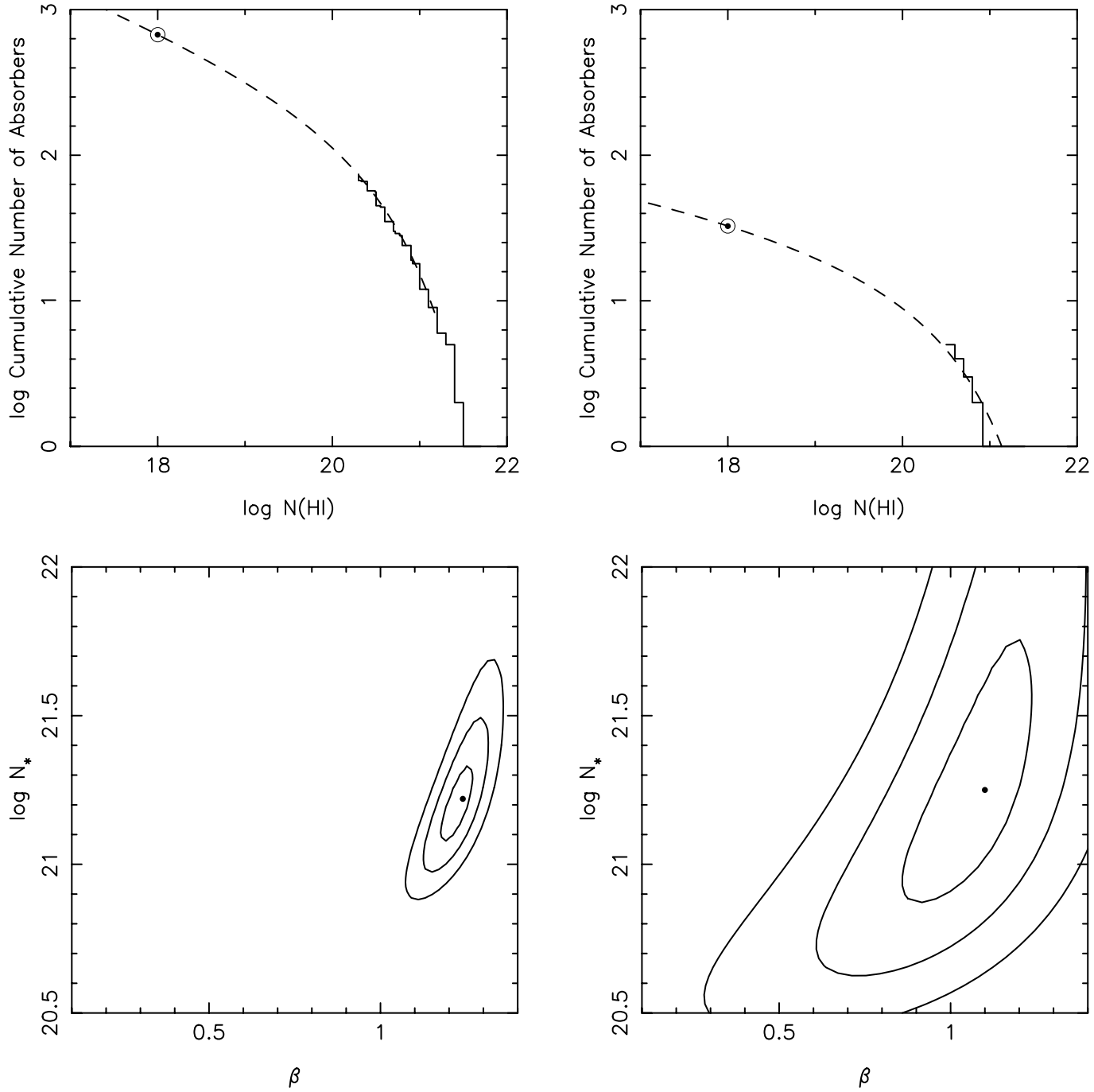

FIG. 10.—*Left*: $1.5 < z < 4.0$; *right*: $z \geq 4.0$. *Top*: The log of the cumulative number of damped Lyα absorbers vs. log column density, including a point for the expected number of Lyman limit systems, shown as a filled circle. The best fits to the column density distribution function of the form $f(N, z) = (f_*/N_*)(N/N_*)^{-\beta} e^{-N/N_*}$ are overplotted using the values in Table 8. *Bottom*: Corresponding >68.3%, >95.5%, and >99.7% confidence contours for the log-likelihood results when calculating β, the slope of the power-law portion of the fit, and log N_*, the knee in the distribution.

4.2. *Number Density Evolution with Redshift*

We now examine the redshift evolution of the damped Lyα absorbers in our combined data set by determining the number density of absorbers per unit redshift, $dN/dz \equiv N(z)$. In a standard Friedmann universe for absorbers with cross sectional area A, absorption distance X, and Φ_0 per unit comoving volume,

$$N(z) = \Phi_0 \, AcH_0 \, \frac{dX}{dz} \, , \tag{6}$$

where

$$\frac{dX}{dz} = \left[\frac{(1+z)^2}{(1+z)^2(1+\Omega_M z) - z(z+2)\Omega_\Lambda} \right]^{1/2} . \tag{7}$$

It is customary to represent the number density as a power law of the form

$$N(z) = N_0(1+z)^\gamma \, . \tag{8}$$

The differential distribution in number density of absorbers versus redshift is shown in Figure 11. It is fitted by a single

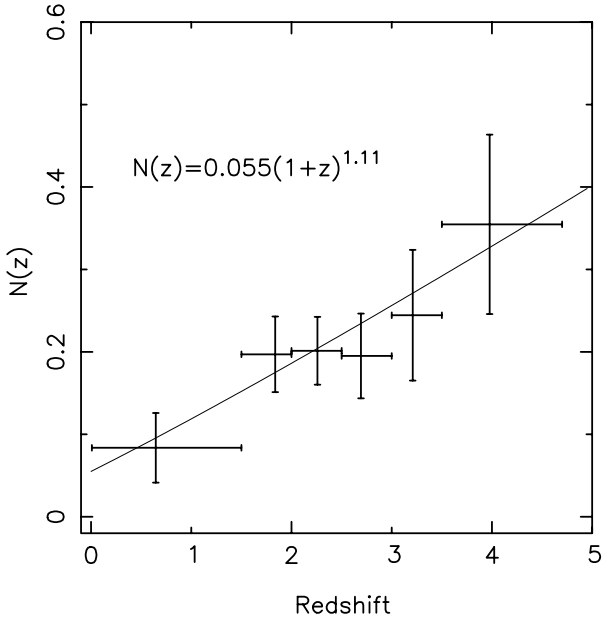

FIG. 11.—Differential distribution in number density of absorbers vs. redshift for the entire data set. It is fitted by a single power law with $N_0 = 0.055$ and $\gamma = 1.11$, which would suggest no intrinsic evolution in the product of the space density and cross section of the absorbers with redshift, but the fit is very poorly constrained, as shown in Fig. 12.

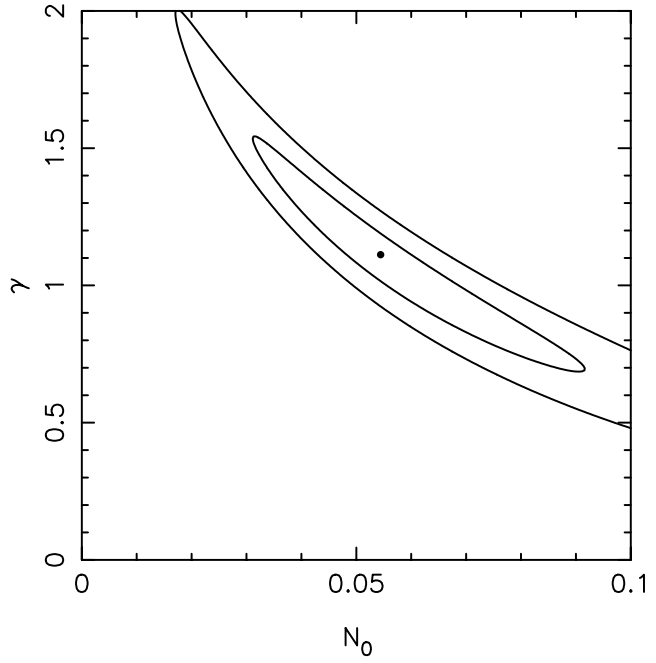

FIG. 12.—Confidence contours >68.3% and >95.5%, plotted for the log-likelihood results for γ and N_0 in fitting the number density per unit redshift with a single power law, $N(z) = N_0(1 + z)^{\gamma}$. The fit for a single power law is very poorly constrained due to differential evolution in the number density of damped Lyα absorbers with different column densities. This is illustrated in Fig. 13.

power law with $N_0 = 0.055$ and $\gamma = 1.11$, which would suggest no intrinsic evolution in the product of the space density and cross section of the absorbers with redshift, but the fit is very poorly constrained. This is evident in the >68.3% and >95.5% confidence contours for the log-likelihood results when calculating γ and N_0, which is shown in Figure 12. The poor fit is due to differential evolution in the number density of damped Lyα absorbers with different column densities, which has been described in LWT95, WLFC95, and SIM96.

The number density of absorbers versus redshift, split at a column density of log $N_{\rm H\,I} = 21$, is shown in Figure 13. The number density of systems with log $N_{\rm H\,I} > 21$, shown as solid lines, peaks at $z \approx 3.5$, when the universe is 15%–20% of its present age. These systems then disappear at a much faster rate from $z = 3.5$ to 0 than does the population of damped absorbers as a whole. There is a paucity of very high column density systems at the highest redshifts surveys, which was also evidenced in the steepening of the column density distribution discussed in § 4.1.3. The number density of damped absorbers with column densities log $N_{\rm H\,I} \leq 21$ decreases from redshifts $z \approx 4$ to $z \approx 3.5$ and remains relatively constant toward $z = 1.5$. The differential evolution with column density suggests:

1. There has been insufficient time at $z > 3.5$ for the highest column density absorbers to collapse.
2. Once they do form, the highest column density absorbers preferentially form stars before their lower column density counterparts, and hence disappear more rapidly toward lower redshifts.

From the evolution of the H I with redshift alone we are unable to determine whether we are watching the evolution of similar systems with redshift or watching some systems disappear and others form.

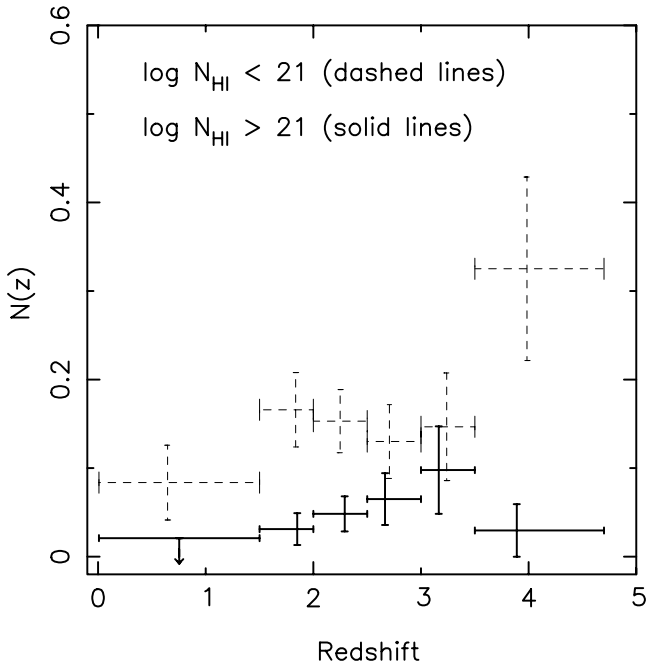

FIG. 13.—Number density per unit redshift, shown for the same data as in Fig. 11, but now split into two groups at a column density of log $N_{\rm H\,I} = 21$. The number density of systems with log $N_{\rm H\,I} > 21$ (*solid lines*), peaks at $z \approx 3.5$, when the universe is 15%–20% of its present age. These systems then disappear at a much faster rate from $z = 3.5$ to $z = 0$ than does the population of damped absorbers as a whole. There is a paucity of very high column density systems at the highest redshift surveys, which was also evidenced in the steepening of the column density distribution discussed in § 4.1.3. The number density per unit redshift of damped absorbers with column densities log $N_{\rm H\,I} \leq 21$ peaks at $z \approx 4$, drops at $z \approx 3.5$, and remains constant or increases slightly toward $z = 1.5$.

4.3. *Evolution of the Mass Density of Neutral Gas*

The comoving mass density of neutral gas is given by

$$\Omega_g(z) = \frac{H_0}{c}\,\frac{\mu m_{\rm H}}{\rho_{\rm crit}}\,\frac{\sum_i N_{\ i}({\rm H\ I})}{\Delta X(z)}\,, \qquad (9)$$

where the density is in units of current critical density (see Lanzetta et al. 1991). The quantity μ is the mean particle mass per $m_{\rm H}$, where $m_{\rm H}$ is the mass of the H atom, $\rho_{\rm crit}$ is the current critical mass density, and the sum is over damped Lyα systems in the statistical sample listed in Table 5. We use $H_0 = 65$ km s^{-1} Mpc in all these calculations. Because we are interested in determining $\Omega_g(z)$ for separate redshift bins, $\Delta X(z)$ is given by the integral $\int g(X)dX$ between the $X(z)$ corresponding to the redshift limits of each bin. We determine $\Omega_g(z)$ by assuming $\mu = 1.3$. The results for our data set from $z = 0.008$ to 4.7 are shown in Figure 14 for three different cosmologies with $\Omega = \Omega_M + \Omega_\Lambda$: (1) $\Omega_M = 1$, $\Omega_\Lambda = 0$; (2) $\Omega_M = 0.3$, $\Omega_\Lambda = 0$; and (3) $\Omega_M = 0.3$, $\Omega_\Lambda = 0.7$. The region Ω_* is the $\pm 1\ \sigma$ range for the mass density in stars in nearby galaxies (Fukugita, Hogan, & Peebles 1998). The point at $z = 0$ is the value inferred from 21 cm emission from local galaxies (Zwaan et al. 1997). These results are tabulated in Table 9. Here Ω_g evolves in the same fashion

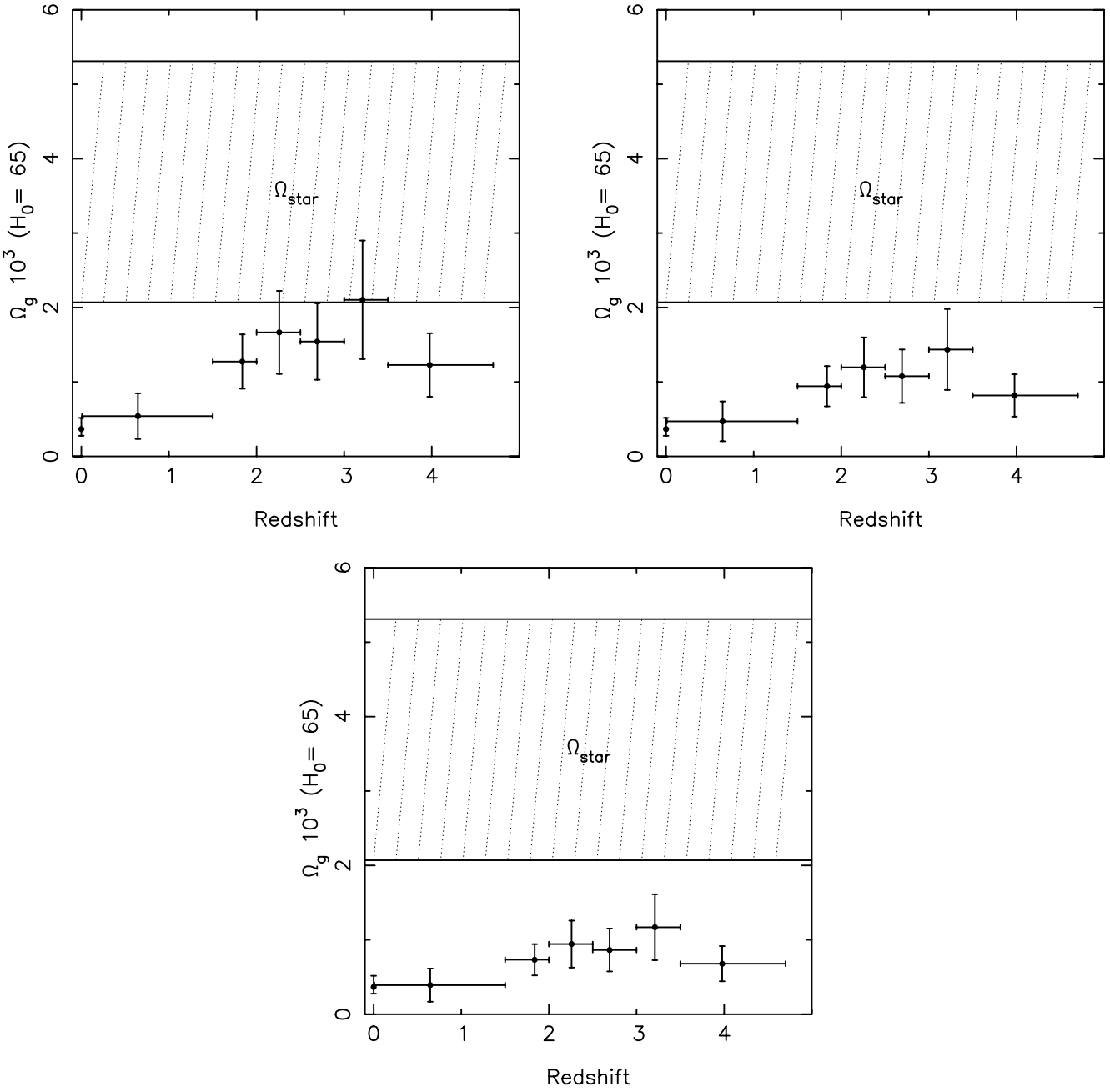

FIG. 14.—Comoving mass density in neutral gas contributed by damped Lyα absorbers, $\Omega_g(z)$, plotted for three different cosmologies: *top left*: $\Omega_M = 1$, $\Omega_\Lambda = 0$; *top right*: $\Omega_M = 0.3$, $\Omega_\Lambda = 0$; and *bottom left*: $\Omega_M = 0.3$, $\Omega_\Lambda = 0.7$. The region Ω_* is the $\pm 1\ \sigma$ range for the mass density in stars in nearby galaxies (Fukugita et al. 1998). The point at $z = 0$ is the value inferred from 21 cm emission from local galaxies (Zwaan et al. 1997). These results are tabulated in Table 9.

TABLE 9

DATA FOR FIGURE 14

			NUMBER OF:		$\Omega = 1, \Lambda = 0$			$\Omega = 0.3, \Lambda = 0$			$\Omega = 0.3, \Lambda = 0.7$		
REDSHIFT RANGE (1)	DLA $\langle z \rangle$ (2)	Δz (3)	DLAs (4)	QSOs (5)	ΔX (6)	Ω_g (7)	σ (8)	ΔX (9)	Ω_g (10)	σ (11)	ΔX (12)	Ω_g (13)	σ (14)
0.008–1.50	0.65	47.8	4	178	58.5	0.54	0.31	67.1	0.47	0.27	80.7	0.39	0.22
1.50–2.00	1.84	96.4	19	372	162.1	1.27	0.36	219.1	0.94	0.27	281.8	0.73	0.21
2.00–2.50	2.26	124.2	25	349	223.0	1.67	0.56	310.3	1.20	0.40	393.7	0.94	0.32
2.50–3.00	2.69	76.9	15	234	148.4	1.54	0.51	212.6	1.08	0.36	265.1	0.86	0.29
3.00–3.50	3.21	40.9	10	128	83.9	2.10	0.80	123.0	1.44	0.54	151.0	1.17	0.44
3.50–4.70	3.98	33.8	12	60	74.5	1.23	0.43	111.8	0.82	0.28	134.6	0.68	0.24

NOTE.—When totalled, the number of QSOs in col. (5) is more than the total for this data set (646). This is because the same QSO can contribute redshift path to more than one redshift bin.

with redshift regardless of the cosmology selected, and there is a tentative peak in Ω_g in the redshift range $3 < z < 3.5$. We consistently find very high column density systems in this redshift range, even though for $z > 4$ QSOs, $z \sim 3$ absorbers are deep in the Lyα forest, where they are most difficult to detect due to the density of the forest lines in the spectra. This was evidenced in § 4.1.1, where the shape of the frequency distribution of column densities was flattest in the $3 < z < 3.5$ redshift bin.

What does change with cosmological model is the ratio of the peak value of Ω_g to Ω_*, the mass density in galaxies in the local universe. We define this ratio as $R_{g*} \equiv \Omega_g(3 < z < 3.5)/\Omega_*$. Previous surveys (Lanzetta et al. 1991; WLFC95; SMI96) have found the value of R_{g*} to be of order 1. When we look at this ratio $[R_{g*} = \Omega_g(z = 3)/\Omega_*]$ for our current data set and value of Ω_*, we find $R_{g*} \approx 0.25$–0.5, depending on the cosmology. For an $\Omega = 1$ universe with a zero cosmological constant, $R_{g*} \approx 0.5$; for an $\Omega = 1$ universe with a positive cosmological constant ($\Omega_\Lambda = 0.7, \Omega_M = 0.3$), $R_{g*} \approx 0.25$; and for a universe with $\Omega_\Lambda = 0$ and $\Omega_M = 0.3$, $R_{g*} \approx 0.3$.

5. DISCUSSION

Although the results for the comoving mass density of neutral gas shown in Figure 14 look very similar to those published in previous work, we here discuss the main differences in these new results and their implications.

1. The values of Ω_g in this work are lower than those previously published for $z > 1.5$. The values for Ω_g published in WLFC95 and SMI96 used $H_0 = 50$ km s^{-1} Mpc, while in this work we use $H_0 = 65$ km s^{-1} Mpc, which decreases Ω_g by 23% at all redshifts. The improved statistics due to the increased redshift path also reduce the effect of the scatter produced by the small number of QSOs with very high column density absorbers. The value of Ω_g is now less sensitive to the maximum column density in any particular redshift bin. The comparison of Ω_g to Ω_* does not appear to be very different, even though the values are lower, because our estimate of Ω_* has changed as well.

2. The value of Ω_* from Fukugita, Peebles, & Hogan (1998) that we use in these plots is also about half the value inferred from Gnedin & Ostriker (1992) used in previous determinations. There are still substantial uncertainties in the relative contributions of disks and spheroids in determining the local mass density (e.g., Salucci & Persic 1999; J. Dalcanton, R. Marzke, & L. Yan 1999, private communication). Salucci & Persic (1999) find a lower value of Ω_* (2×10^{-3}) independent of the Hubble constant, which is about half the value we have plotted from Fukugita et al. (1998). As our understanding of the local mass density improves, we will continue to refine these numbers for comparison with the high-redshift determinations.

3. The calculation of Ω_g for $z > 3.5$ in SMI96 hinted at a turnover at these high redshifts. Our larger data set does not confirm whether or not this turnover is real, although the trend continues to be present in our larger data set. We do see a statistically significant change in the frequency distribution of column densities at $z > 4$ (§ 4.1.3), which suggests that we are probing an epoch at which the highest column density absorbers have not yet collapsed. In addition, for one of the highest column density high-redshift systems (log $N_{\rm H\,I} \leq 21.1$ at $z = 3.89$) from PC 0953+4749,

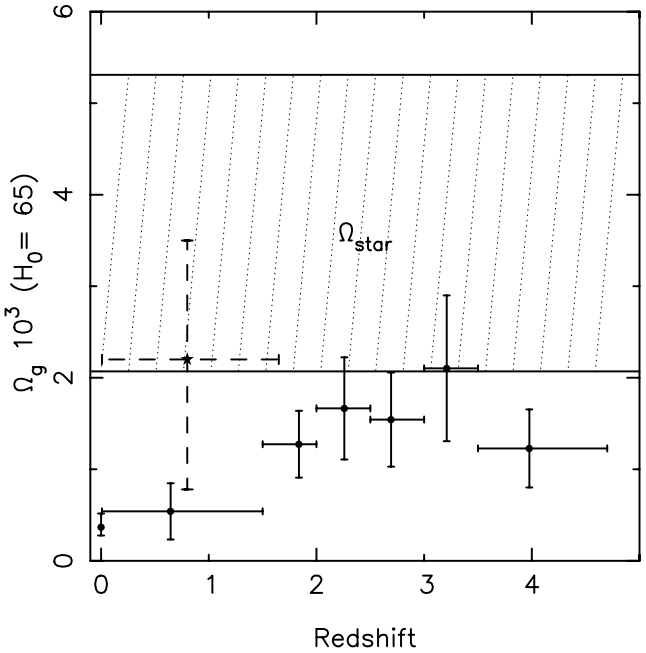

FIG. 15.—Same as top left panel ($\Omega_M = 1, \Omega_\Lambda = 0$) of Fig. 14, showing the comoving mass density in neutral gas contributed by damped Lyα absorbers, $\Omega_g(z)$, with the value from Rao & Turnshek (2000) for $z < 1.65$ plotted as dashed lines. The error bars are still very large, but they find a substantially higher value of Ω_g at lower redshifts than indicated from previous surveys.

we only have an upper limit for the column density, as discussed in § 2.1.1. Although we have surveyed enough quasars at $z > 3.5$ not to be extremely sensitive to the inclusion or exclusion of one absorber, it is true that if this high column density were substantially lower, the error bars for the $3 < z < 3.5$ and $z > 3.5$ bins would not overlap. We will have to wait for more data to make a definitive statement about a turnover in Ω_g at $z > 4$.

4. The Ω_g determined in WLFC95 shows a monotonic decrease from $z = 3.5$ to 0.008. Our larger data set also shows a decrease, but the inclusion of the addition survey of Storrie-Lombardi & Hook (2000) makes Ω_g flatter in the redshift range $2 < z < 3$. Our new data are consistent with a constant value of Ω_g for $2 < z < 4$. New results from Rao & Turnshek (2000) for $z < 1.5$ also suggest that Ω_g ($z < 1.5$) may be higher than previously determined. In Figure 15 we replot the first panel of Figure 14, and show their lower redshift data point with dashed lines. The error bars are still very large, but they find a substantially higher value for Ω_g at $z < 1.65$ than previous surveys.

We thank Julia Kennefick, George Djorgovski, Mike Irwin, and Richard McMahon for providing QSO coordinates prior to publication and the staff at Keck, Lick, and the AAT for their able assistance in obtaining these observations. L. S. L. thanks Jason Prochaska, Celine Peroux, and Max Pettini, and an anonymous referee for helpful suggestions.

REFERENCES

Bahcall, J. N., & Peebles, P. J. E. 1969, ApJ, 156, L7
Black, J. H., Chaffee, F. H., & Foltz, C. B. 1987, ApJ, 317, 442
Fall, S. M., & Pei, Y. C. 1993, ApJ, 402, 479
Francis, P. J., & Hewett, P. C. 1993, AJ, 106, 2587
Fukugita, M., Hogan, C. J., & Peebles, P. J. E. 1998, ApJ, 503, 518
Gnedin, N. Y., & Ostriker, J. P. 1992, ApJ, 400, 1
Haehnelt, M. G., Steinmetz, M., & Rauch, M. 1998, ApJ, 495, 647
Hu, E. M., Kim, T., Cowie, L. L., Songaila, A., & Rauch, M. 1995, AJ, 110, 1526
Jannuzi, B. T., et al. 1998, ApJS, 118, 1
Kennefick, J. D., de Carvalho, R. R., Djorgovski, S. G., Wilber, M. M., Dickson, E. S., Weir, N., Fayyad, U., & Roden, J. 1995, AJ, 110, 78
Lanzetta, K. M. 1991, ApJ, 375, 1
Lanzetta, K. M., Wolfe, A. M., & Turnshek, D. A. 1995, ApJ, 440, 435 (LWT95)
Lanzetta, K. M., Wolfe, A. M., Turnshek, D. A., Lu, L., McMahon, R. G., & Hazard, C. 1991, ApJS, 77, 1
Le Brun, V., Bergeron, J., Boisse, P., & Deharveng, J. M. 1997, A&A, 321, 733
Lu, L., Sargent, W. L. W., Womble, D. S., & Barlow, T. A. 1996, ApJ, 457, L1
Lu, L., & Wolfe, A. M. 1994, AJ, 108, 44
Lu, L., Wolfe, A. M., Turnshek, D. A., & Lanzetta, K. M. 1993, ApJS, 84, 1
McMahon, R. G., Omont, A., Bergeron, J., Kreysa, E., & Haslam, C. G. T. 1994, MNRAS, 267, L9
Oke, J. B., et al. 1995, PASP, 107, 375
Pei, Y. C., & Fall, S. M. 1995, ApJ, 454, 69
Pei, Y. C., Fall, S. M., & Hauser, M. G. 1999, ApJ, 522, 604
Petitjean, P., Webb, J. K., Rauch, M., Carswell, R. F., & Lanzetta, K. M. 1993, MNRAS, 262, 499
Pettini, M., Ellison, S. L., Steidel, C. C., & Bowen, D. V. 1999, ApJ, 510, 576
Pettini, M., Smith, L. J., Hunstead, R. W., & King, D. L. 1994, ApJ, 426, 79
Pettini, M., Smith, L. J., King, D. L., & Hunstead, R. W. 1997, ApJ, 486, 665
Prochaska, J. X., & Wolfe, A. M. 1997, ApJ, 487, 73
———. 1998a, ApJ, 494, L15
———. 1998b, ApJ, 507, 113
Prochaska, J. X., & Wolfe, A. M. 1999, ApJS, 121, 369
Rao, S., & Briggs, F. 1993, ApJ, 419, 515
Rao, S. M., & Turnshek, D. A. 1998, ApJ, 500, L115
———. 2000, ApJ, in press
Rauch, M., Carswell, R. F., Robertson, G. G., Shaver, P. A., & Webb, J. K. 1990, MNRAS, 242, 698
Salucci, P., & Persic, M. 1999, MNRAS, 309, 923
Sargent, W. L. W., Steidel, C. C., & Boksenberg, A. 1988, ApJ, 334, 22
———. 1989, ApJS, 69, 703
Savaglio, S., D'Odorico, S., & Moller, P. 1994, A&A, 281, 331
Schechter, P. 1976, ApJ, 203, 297
Schneider, D. P., Schmidt, M., & Gunn, J. E. 1987, ApJ, 316, L1
———. 1989, AJ, 98, 1507
———. 1991, AJ, 101, 2004
Stengler-Larrea, E. A., et al. 1995, ApJ, 444, 64
Storrie-Lombardi, L. J., & Hook, I. M. 2000, ApJS, submitted
Storrie-Lombardi, L. J., Irwin, M. J., & McMahon, R. G. 1996a, MNRAS, 282, 1330 (SIM96)
Storrie-Lombardi, L. J., McMahon, R. G., & Irwin, M. J. 1996b, MNRAS, 283, L79 (SMI96)
Storrie-Lombardi, L. J., McMahon, R. G., Irwin, M. J., & Hazard, C. 1994, ApJ, 427, L13
———. 1996, ApJ, 468, 121 (SMIH96)
Turnshek, D. A., Wolfe, A. M., Lanzetta, K. M., Briggs, F. H., Cohen, R. D., Foltz, C. B., Smith, H. E., & Wilkes, B. J. 1989, ApJ, 344, 567
Tytler, D. 1982, Nature, 298, 427
———. 1987, ApJ, 321, 49
Warren, S. J., Hewett, P. S., & Osmer P. S. 1991, ApJS, 76, 23
White, R. L., Kinney, A., & Becker, R. H. 1993, ApJ, 407, 456
Wolfe, A. M., Lanzetta, K. M., Foltz C. B., & Chaffee, F. H. 1995, ApJ, 454, 698 (WLFC95)
Wolfe, A. M., Turnshek, D. A., Lanzetta, K. M., & Lu, L. 1993, ApJ, 404, 480
Wolfe, A. M., Turnshek, D. A., Smith, H. E., & Cohen, R. D. 1986, ApJS, 61, 249
Zwaan, M. A., Briggs, F. H., Sprayberry, D., & Sorar, E. 1997, ApJ, 490, 173